Quaternary Science Reviews 87 (2014) 98–113

Contents lists available at ScienceDirect

Quaternary Science Reviews

journal homepage: www.elsevier.com/locate/quascirev

A 31,000 year record of paleoenvironmental and lake-level change from Harding Lake, Alaska, USA

Matthew S. Finkenbinder [a,*], Mark B. Abbott [a], Mary E. Edwards [b,c], Catherine T. Langdon [b], Byron A. Steinman [d], Bruce P. Finney [e,f]

[a] Geology and Planetary Science, University of Pittsburgh, Pittsburgh, PA 15260, USA
[b] Geography and Environment, University of Southampton, Highfield, Southampton SO17 1BJ, UK
[c] Alaska Quaternary Center, University of Alaska-Fairbanks, Fairbanks, AK 99775, USA
[d] Department of Meteorology and Earth and Environmental Systems Institute, Pennsylvania State University, University Park, PA 16802, USA
[e] Department of Biological Sciences, Idaho State University, Pocatello, ID 83209, USA
[f] Department of Geosciences, Idaho State University, Pocatello, ID 83209, USA

ARTICLE INFO

Article history:
Received 5 September 2013
Received in revised form
2 January 2014
Accepted 4 January 2014
Available online

Keywords:
Lake sediment geochemistry
Alaska
Late-Quaternary
Paleolimnology
Climate change
Lake-level

ABSTRACT

Physical and geochemical proxy analyses of sediment cores from Harding Lake in central Alaska are used to reconstruct paleoenvironmental change and millennial scale fluctuations in lake level for the last ~31,000 years. We analyzed a composite 422 cm core from the lake depocenter (42.1 m water depth) and identified 4 distinct lithologic units based on variability in dry bulk density, organic matter, biogenic silica, carbon to nitrogen mass ratios (C/N), organic matter carbon isotopes ($\delta^{13}C$), pollen, and elemental abundances via scanning X-ray fluorescence, with age control provided by 16 Accelerator Mass Spectrometry radiocarbon dates and ^{210}Pb dating. In addition, we analyzed a transect of cores from 7.1 m, 10.75 m, 15.91 m, and 38.05 m water depths to identify lake level fluctuations and to characterize sediment compositional changes as a function of water depth. Organic matter content and magnetic susceptibility values in surface sediments from all transect cores show a strong correlation with water depth. Interpretation of four lithologic units with well-dated contacts produced a record of water-depth variations that is consistent with independent climate records from eastern Beringia. Basal coarse-grained sediments (quartz pebble diamicton) were deposited prior to 30,700 calendar years before present (yr BP), possibly from fluvial reworking or deflation during a period of severe aridity. Unit 1 sediments were deposited between 30,700 and 15,700 yr BP and are characterized by a low organic matter content, a high magnetic susceptibility, and low biogenic silica concentrations resulting from very low lake levels, low terrestrial and in-lake productivity and a high flux of clastic sediment. An abrupt increase in organic matter and biogenic silica concentration marks the transition into Unit 2 sediments, which were deposited between 15,700 and 9,400 yr BP when lake levels were higher and variable (relative to Unit 1). The transition to full interglacial conditions at 9,400 yr BP marks the beginning of Unit 3. Here an abrupt increase in the sedimentation rate, organic matter and biogenic silica concentration occurs (along with a corresponding decrease to low magnetic susceptibility). These high values persist until 8,700 yr BP, signifying a rapid rise to higher lake levels (in comparison to Units 1 and 2). Unit 4 sediments were deposited between 8,700 yr BP to 2010 AD and generally contain high concentrations of organic matter and biogenic silica with low magnetic susceptibility, suggesting that lake levels were relatively high and stable during the middle to late Holocene.

1. Introduction

The Tanana valley in the interior of Alaska, encompassing the broad unglaciated lowland of eastern Beringia (Péwé, 1975) remained ice-free during the Last Glacial Maximum (LGM; 26,500–19,000 calendar years before present [yr BP]). Regionally, glaciers were restricted to the Alaska Range to the south and the Yukon-Tanana Uplands to the north (Coulter et al., 1965). Evidence suggests much colder, drier, and windier conditions than at present occurred during the LGM (Hopkins, 1982). However, these observations from interior Alaska, based on investigation of loess (Muhs et al., 2003), frozen silt and permafrost (Hamilton et al., 1988), lake

* Corresponding author.
E-mail address: msf34@pitt.edu (M.S. Finkenbinder).

0277-3791/$ – see front matter © 2014 Elsevier Ltd. All rights reserved.
http://dx.doi.org/10.1016/j.quascirev.2014.01.005

sediments (Nakao and Ager, 1985), and an alluvial basin (Matthews, 1974) are poorly resolved, discontinuous, and beset by chronological problems. For example, analysis of drilled cores from Harding Lake (analyzed at sub-millennial scale resolution for pollen and radiocarbon dated using bulk sediments) reveal an age reversal at the core bottom but suggest lacustrine sediments span the last 26,500 ± 400 ^{14}C years (Nakao and Ager, 1985). Several lake records with basal ages of ~15,000 yr BP from this region (Ager, 1975, 1983; Abbott et al., 2000; Bigelow and Edwards, 2001; Carlson and Finney, 2004) indicate substantial climatic change during the Lateglacial period with increases in temperature and effective moisture (precipitation minus evaporation). Cosmogenic exposure (CE) dating of moraines has yielded several late Pleistocene glacial records indicating the LGM glacial maxima occurred between 16,000 and 17,000 yr BP on the north slope of the Alaska Range (Young et al., 2009; Matmon et al., 2010) and between 21,000 and 23,000 yr BP in the Yukon-Tanana Uplands (Briner et al., 2005). While helpful, these records of moraine stabilization offer only 'snap-shot' views of paleoclimate and are of limited utility in documenting paleoclimatic conditions between dated glacier advances. Given the lack of continuous, well-dated paleoclimate records spanning the LGM in interior Alaska and the need for records against which to compare paleoclimate model simulations (eg. Otto-Bliesner et al., 2006), additional work is necessary to investigate the timing and magnitude of late Quaternary climatic change and the resulting paleoenvironmental effects in central Alaska.

In this study, we present a ~31,000 year record of paleoenvironmental change inferred from analyses of overlapping sediment cores from Harding Lake. We analyzed multiple physical and geochemical proxies (including dry bulk density, organic matter, biogenic silica, carbon to nitrogen mass ratios (C/N), bulk sediment organic matter carbon isotopes (δ^{13}C), pollen, and elemental abundances via scanning X-ray fluorescence), using Accelerator Mass Spectrometry (AMS) radiocarbon and a surface ^{210}Pb profile to establish age control. The Harding Lake sedimentary record continuously spans the period prior to the LGM through to the present. In addition, we analyzed a depth transect of cores from 7.1 m, 10.75 m, 15.91 m, and 38.05 m water depths to track lake-level fluctuations and to characterize shallow water sediments. We compare the Harding Lake record to other regional glacial and lacustrine records to examine the timing of paleoenvironmental responses to insolation forcing and the climatic effects of the exposure and later submergence of the Bering and Chukchi continental shelves during the late Pleistocene and earliest Holocene.

2. Study site and regional setting

Harding Lake (64.42° N, 146.85° W; 217 m ASL) is located in the interior of central Alaska in the Tanana valley, approximately 60 km southeast of Fairbanks (Fig. 1). The maximum and mean water depths are 43 m and 16 m, respectively. The lake has a surface area of 9.88 km^2 and a watershed area of roughly 20 km^2 (LaPerriere, 2003). Harding Lake is oligotrophic and usually dimictic, with overturning and mixing occurring in the spring and fall (LaPerriere, 2003). Infrequently spring overturn events do not occur, leading to meromixis during these years. Water quality data collected in March 2010 from core site D-10 (Fig. 1) reveal thermal and chemical stratification of the water column (Fig. 2). Surface lake water had a temperature of 0.5° C, a specific conductivity of 0.102 μS/cm, a pH of 7.13, and dissolved oxygen of 12.95 mg/L. The oxygen (δ^{18}O) and hydrogen (δD) isotopic values of lake water collected in July, 1996 were −12.59‰ and −116.91‰ (VSMOW), respectively. Water isotope data from several lakes and rivers in the Tanana Valley (Wooller et al., 2012) show that Harding Lake water isotopic values plot along the regional evaporation line, indicating that water loss via evaporation is a considerable flux in the lake hydrologic budget.

Surface inflow to the lake periodically occurs from the outflow of Little Harding Lake (0.18 km^2 lake surface area, 2.88 km^2 watershed area) to the southwest and a small stream on the northeastern shore. Harding is a topographically closed-basin lake with respect to surface outflow. Lake levels are primarily controlled by variations in the balance between evaporation and precipitation falling directly on the lake surface, because of the small watershed size (relative to the lake surface area) and the lack of a surface outflow. Variability in lake levels have been noted in the recent past; for example, low lake levels in the 1930's and early 1970's were followed by higher lake levels in late 1970's and early 1980's (LaPerriere, 2003). During times of low lake level, the shallow shelf at the northern edge of Harding Lake is exposed. Review of historical aerial photos shows a relatively higher lake level in 1978 and relatively lower lake levels in 1996 and 2003. Quantitative assessments of historical lake level changes are not available; however, frequent exposure and submergence of the shelf along the northern shore suggests fluctuations on the scale of a few meters.

Harding Lake is located at the southern edge of the Yukon-Tanana Uplands Physiographic Province, which is characterized by rounded, gentle relief ridges and broad interfluves (Wahrhaftig, 1965). Tributary streams in the southern portion flow south into the Tanana River, including the Salcha River located north of Harding Lake. Bedrock geology in the watershed consists of medium to high grade pelitic schist (Wilson et al., 1998) with few exposures. The majority of the landscape and low-relief hills to the south and east of Harding Lake are mantled with loess (Blackwell, 1965). Extensive sand dune and loess deposits exist throughout the Tanana River Valley in the Fairbanks area (Péwé, 1975) along with discontinuous permafrost (Jorgenson et al., 2008). Blackwell (1965) attributed the origin of Harding Lake to aggradation of Tanana River during the Delta Glaciation (penultimate) and damming of a tributary flowing south from the Yukon-Tanana Uplands. The formation of several other lakes abutting the Yukon-Tanana Uplands, including Birch Lake, Quartz Lake, and Chisholm Lake, are hypothesized to result from the same process. Nakao et al. (1981) conducted a gravimetric survey from the surface of Harding and Little Harding Lake and suggested that a fault valley and trough exists underneath the area. They concluded the lake formed as a result of tectonic activity and faulting, and the subsequent damming of a small tributary resulting from aggradation of the Tanana River (Nakao et al., 1981).

The regional climate is classified as Interior (Sub-Arctic), with maximum summer temperatures above 30 °C and minimum winter temperatures below −40 °C (Stafford et al., 2000). Climate data from Fairbanks International Airport (Fig. 2; 64.818° N, 146.863° W; 135 m ASL; 1948–2010 AD) reveal average winter (January–February–March) and summer (June–July–August) temperatures of −18 °C and 15.2 °C, respectively. The Interior is bounded by the Brooks Range to the north and Alaska Range to the south, which produce significant orographic barriers to moisture transport leading to annual precipitation values ranging from 200 to 400 mm (Stafford et al., 2000). Numerous studies suggest the location and strength of the Aleutian Low and Siberian/Beaufort High pressure cells have a strong influence on atmospheric circulation and temperature and precipitation patterns in interior Alaska (Mock et al., 1998; Cassano et al., 2011). Specifically, warmer temperatures occur when the Aleutian Low is strong and located over the Aleutian Islands, a scenario that produces a southerly air mass trajectory (Cassano et al., 2011). Colder temperatures result when low pressure systems are positioned to the southwest of the Aleutian Islands and over the Canadian Archipelago, along with an area of high pressure centered over eastern Siberia (Siberian High).

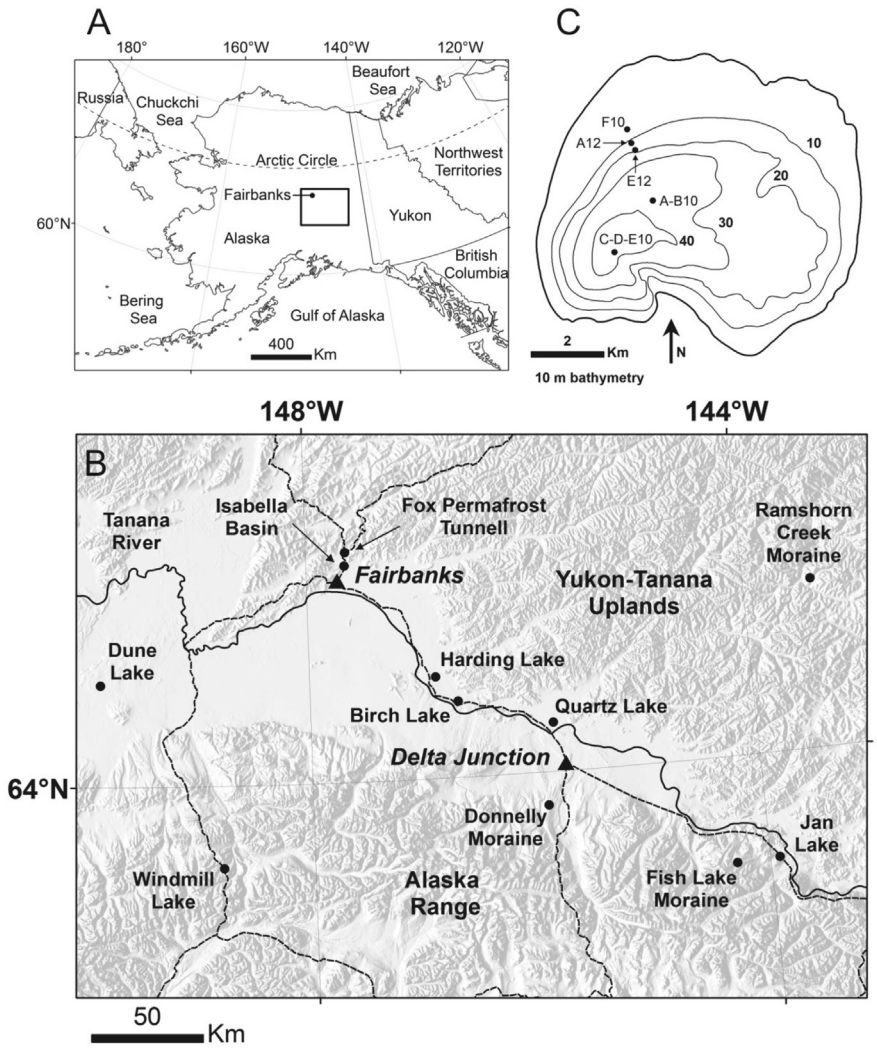

Fig. 1. A) Regional site location map of Alaska and the surrounding area. B) Shaded relief map of the Harding Lake area with sites mentioned in the text. Dashed lines are major roads and solid lines are major rivers. C) Bathymetric map of Harding Lake showing 10 m depth contours and core sites (modified from Nakao and Ager, 1985).

Positive precipitation anomalies (wet conditions) are associated with a weakened Aleutian Low positioned to the west over the Aleutian Islands. In contrast, negative precipitation anomalies (dry conditions) typically occur when the Aleutian Low is in a more easterly position in the Gulf of Alaska, a configuration that produces more southerly winds and less moisture delivery across the Alaska Range into the interior (Streten, 1974). The above synoptic climate controls are more important for winter conditions due to their association with the Aleutian Low pressure system, which is stronger in winter months. In contrast, summer climate is more influenced by mid-tropospheric variations of ridges and troughs (Streten, 1974) that control atmospheric circulation and the resultant trajectory of air masses traveling to the interior. Instrumental weather data from Fairbanks (Fig. 2) and across interior Alaska indicate the majority of annual precipitation occurs during summer months, with peak values typically occurring in July and August.

3. Methods

3.1. Sediment coring

Sediment cores were collected through the ice from multiple locations on Harding Lake in March, 2010 (Fig. 1). A surface core (D-10) with intact sediment–water interface was recovered from 42.1 m water depth using a UWITEC surface corer. Upon recovery, the flocculate upper portion of the sediment was extruded in the field at 0.5 cm intervals to a depth of 34 cm. Multiple overlapping long cores were recovered from core sites A-10 and B-10 in 38.05 m water (64.422° N, 146.854° W), and C-10, D-10, and E-10 in 42.1 m water (64.419° N, 146.858° W) using a 9 cm diameter UWITEC percussion coring system. Core F-10 (64.425° N, 146.857° W) was recovered from 7.1 m water depth using a square rod Livingston corer. To better characterize shallow and intermediate water depth sediments and to track lake-level fluctuations, two additional cores were recovered from an inflatable raft in July, 2012 (Fig. 1). Core A-12 (64.425° N, 146.856° W) was recovered from 10.75 m water depth and core E-12 (64.424° N, 146.856° W) from 15.91 m water depth using a square rod Livingston corer. After recovery, all long cores were sealed in plastic, capped, wrapped with duct tape, and transported to the Department of Geology and Planetary Science at the University of Pittsburgh.

3.2. Geochronology

The composite core age model was developed from ^{210}Pb dating of surface sediments and AMS radiocarbon analyses of 16 terrestrial

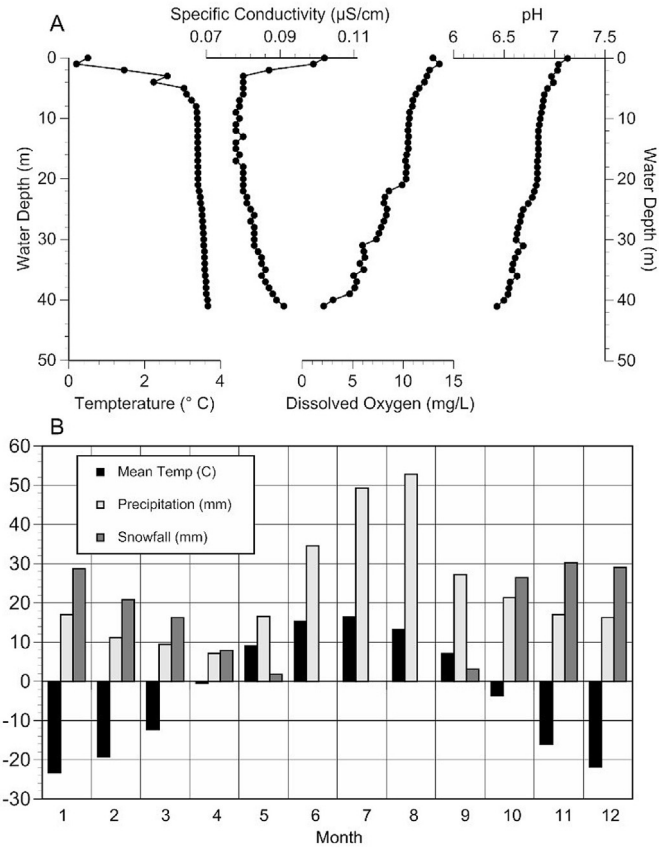

Fig. 2. A) Physical water quality data from the Harding Lake water column at core site D-10 (collected in March, 2010) and B) Average monthly weather data from Fairbanks International Airport for the period 1948–2010 AD.

macrofossils (Table 1). Freeze dried and homogenized aliquots of the top 15 cm of surface core D-10 were analyzed for radioisotope (^{210}Pb, ^{214}Pb, ^{137}Cs and ^{226}Ra) activities by direct gamma counting using a high purity germanium detector (Canberra model BE-3825) with a closed-end coaxial well located in the Department of Geology and Planetary Science at the University of Pittsburgh. Detector efficiency was determined by counting a Canberra MGS-1 multi-gamma standard for which peak efficiencies have been established using a National Institute of Standards traceable standard. Excess ^{210}Pb activities were calculated by subtracting the background ^{214}Pb activity, sourced from in-situ decay of ^{226}Ra within the sediment matrix, from the ^{210}Pb activity sourced from direct atmospheric deposition. Sediment ages were calculated using the Constant Rate of Supply (CRS) method, which accounts for variability in both the sedimentation rate and dry bulk density, according to the methodology of Binford (1990). Bulk sediment samples were disaggregated and wet-sieved to separate terrestrial macrofossils for AMS radiocarbon measurement. Organic samples were pre-treated using standard acid–base–acid wash techniques (Abbott and Stafford, 1996) and were combusted, graphitized, and measured at the W.M. Keck Carbon Cycle AMS Laboratory, University of California, Irvine. Radiocarbon ages were calibrated to calendar years BP (1950) using CALIB 6.0 and the INTCAL09 calibration curve (Reimer et al., 2009). Radiocarbon samples from charcoal, wood, plant material, and seeds (Table 1) were analyzed from the composite core. An age-depth model was created using point to point, linear interpolation with the classical age modeling (CLAM) code for the statistical software R (Blaauw, 2010). In addition, one radiocarbon sample from core A-12 and three samples from core E-12 (Table 1) were analyzed to constrain the timing of sediment deposition and subsequent lake-level fluctuations at each core site.

Table 1
AMS Radiocarbon dates with calibrated 2 sigma error ranges. Samples highlighted with an asterisk are stratigraphically reversed and not included in the depth to age model.

Sample ID (UCIAMS #)	Core-drive	Total depth (cm)	Material	Raw age (^{14}C yr BP)	Error (yr)	Calib age (2σ) (yr BP)
Core C-10/E-10 composite						
89203	C10-D1	22.5	Charcoal	380	30	319–505
109356	C10-D1	36.5	Charcoal	1,245	25	1,082–1,267
89204	C10-D1	46.5	Wood	1,570	40	1,375–1,541
89205	C10-D1	65.0	Seeds	2,700	15	2,761–2,844
89206	C10-D1	101.0	Wood	4,160	45	4,538–4,834
89207	C10-D1	165.0	Charcoal	6,960	70	7,673–7,935
89208	C10-D2	195.5	Charcoal	8,000	100	8,585–9,134
89209	C10-D2	200.5	Charcoal	8,130	60	8,795–9,285
89210	E10-D2	277.5	Charcoal	8,450	80	9,272–9,550
89211	E10-D2	281.0	Charcoal	8,820	160	9,537–10,233
109357	E10-D2	302.5	Charcoal	10,310	160	11,407–12,577
109358	E10-D2	320.5	Plant material	10,690	190	12,059–13,068
* 109359	E10-D2	351.5	Seeds	8,770	370	8,787–11,065
89212	E10-D2	362.5	Wood	13,560	100	16,359–16,967
* 109360	E10-D2	383.5	Plant material	10,740	310	11,643–13,285
89213	E10-D2	412.5	Charcoal	25,900	320	29,848–31,193
Core A-12						
131490	A12-D1	73.5	Seed	12,670	380	13,854–16,526
Core E-12						
131489	E12-D1	93.5	Wood	8,650	100	9,468–10,119
131489	E12-D2	118.5	Wood	11,820	300	13,093–14,841
116879	E12-D2	120.5	Wood	12,175	35	13,872–14,174

3.3. Lithostratigraphy

Sediment cores were split, described, and photographed at the Department of Geology and Planetary Science at the University of Pittsburgh. Notable sedimentary structures, grain-size, and Munsell color were characterized for each core. A composite depth scale of 422 cm was created with surface core D-10, and long cores C-10 Drive 1, D-10 Drive 1, C-10 Drive 2, and E-10 Drive 2 based on anomaly matching proxy data (Fig. 3) and visible stratigraphic markers. Thirty, 1 cm samples (spanning the entirety of the composite record) were analyzed via smear-slide mineralogy and described according to the lacustrine sediment classification scheme of Schnurrenberger et al. (2003). Dry bulk density and weight percent organic matter values were measured on all cores at continuous 1 cm intervals via loss-on-ignition (LOI) at 550 °C for 4 h (Heiri et al., 2001). Magnetic susceptibility was measured on all split cores at 2 mm intervals using a Bartington MS2 Magnetic Susceptibility Meter.

Weight percent Biogenic Silica (BSi) was measured at 2 cm intervals on 209 samples (including 20 replicates) from the composite core using a wet-chemistry, alkaline extraction adapted from Mortlock and Froelich (1989). Prior to analysis wet samples were freeze-dried, homogenized to a fine powder, and treated with 30% H_2O_2 and 1 M HCl to remove organic matter and carbonate minerals, respectively. BSi was extracted with a 10% Na_2CO_3 solution and determined by molybdate blue spectrophotometry at 812 nm (Mortlock and Froelich, 1989) using a Thermo Scientific Evolution 60s UV–Visible Spectrophotometer. Replicate measurements of internal sediment standards from Laguna de Los Anteojos (Stansell et al., 2010) run during sample analysis produced an average error of 3.1%.

Carbon to nitrogen mass ratios (C/N) and bulk sediment organic matter stable isotopes of carbon (δ^{13}C) were measured at 1 cm intervals from 0 to 25 cm and at 2 cm intervals over the remainder of the composite core at the Stable Isotope Laboratory at Idaho State

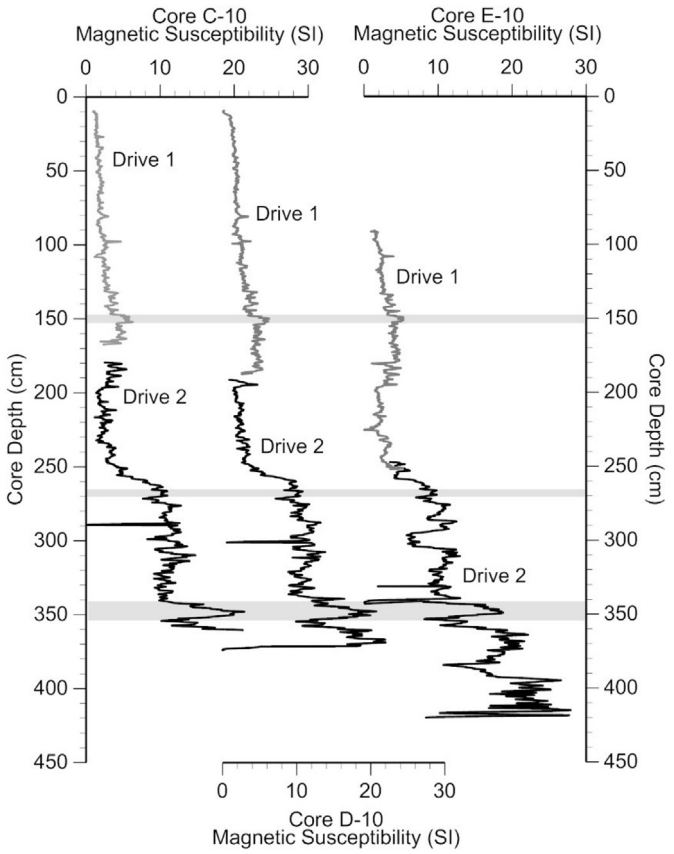

Fig. 3. Magnetic susceptibility for cores C-10, D-10, and E-10 recovered from 42.1 m water depth showing the anomaly match used to construct the 422 cm composite depth scale. Gray bars indicate the major anomalies present in each core.

University. Total organic carbon (TOC), total nitrogen (TN), and organic matter $\delta^{13}C$ measurements were obtained using an Elemental Combustion System 4010 interfaced to a Delta V Advantage mass spectrometer through the ConFlo IV system. Samples were treated with 1 M HCl to remove carbonate minerals and subsequently freeze-dried and homogenized prior to analysis. The mass ratio of TOC to TN (C/N) was calculated to assess organic matter sources. Values of $\delta^{13}C$ are reported as ‰ values relative to the VPDB scale. Replicate measurements of internal standards yielded coefficients of variation of 1.4% and 1.5% for total organic carbon and total nitrogen, and precision better than 0.15‰ for the stable isotope measurements.

Bulk sediment geochemistry was measured continuously at 1 cm intervals with 60 s count times on the split composite cores using the ITRAX X-ray fluorescence (XRF) core scanner at the Large Lakes Observatory, University of Minnesota Duluth. The D-10 D1 core was not scanned because an earlier composite depth scale based on field measurements did not include this drive. As a result, an 11 cm gap in XRF data exists in the composite depth scale (168–179 cm) where core D-10 D1 spans the overlap between core C-10 D1 and C-10 D2. The ITRAX XRF provides a non-destructive, high resolution and semi-quantitative record of elemental abundances (Croudace et al., 2006). Values are reported as counts per second. We focus our paleoenvironmental interpretation on titanium concentrations, which are typically used as proxy for detrital clastic flux (eg. Balascio and Bradley, 2012).

Pollen analysis was carried out at approximately 20 cm intervals through the upper 350 cm and approximately 10 cm intervals through the basal 80 cm of the composite core. We used conventional methodologies for preparation, identification, and counting (Faegri et al., 1989), plus heavy-liquid separation (sodium polytungstate; Elias et al., 1999) and extra sieving for silt- and sand-rich samples. The pollen sum was typically ≥300 terrestrial pollen grains, excluding spores and aquatic taxa, but lower in the inorganic basal 80 cm. Pollen reference material held at the University Southampton was consulted when necessary. The pollen diagram was plotted using TILIA software (Grimm, 1990).

4. Results and interpretations

4.1. Sediment core geochronology

The composite core sedimentology and depth to age model, based on 16 AMS radiocarbon dates and the ^{210}Pb profile (as well as linear sedimentation rates (cm/yr)) are presented in Fig. 4. Two samples (UCIAMS # 109359 and # 109360) produced stratigraphic age reversals and were excluded prior to generating the age model. The first sample (UCIAMS # 109359, at 351.5 cm) was a seed that yielded an extremely small carbon yield (10 μg) and very large analytical uncertainty (Table 1). The second sample (UCIAMS # 109360, at 383.5 cm) was plant material that also yielded a small carbon yield (17 μg) and large analytical uncertainty (Table 1). Inclusion of either of these dates would necessitate rejecting other radiocarbon measurements from much larger samples with smaller analytical uncertainty. The exact cause of these age discrepancies is unknown, however we hypothesize the very small Carbon yields, which are near the threshold limit for AMS radiocarbon analysis at UCI KCCAMS, are the most likely source of error. For example, the influence of modern carbon contamination through sample processing (e.g. pretreatment, combustion, and graphitization) increases with decreasing sample size for radiocarbon analysis (Santos et al., 2010). In an investigation of the effects of sample mass on radiocarbon dates from Arctic lake sediments, Oswald et al. (2005) found that ages for samples of >50 μg carbon from the same macrofossil produced statistically indistinguishable ages. However, ages for samples of <50 μg carbon were substantially younger and had greater uncertainty, which they attributed to the combined effects of incomplete graphitization and a larger influence from background contamination. As a result, we consider the reported ages of the samples at 351.5 cm and 383.5 cm (UCIAMS # 109359 and # 109360) to be too young given more robust, adjacent dates and therefore reject both from the age model.

Sedimentation rates, calculated as sediment accumulation per unit time (cm/year), reveal considerable temporal variability in sediment deposition (Fig. 4). Sedimentation rates were extremely low (0.004 cm/yr) from 30,700 yr BP to 16,800 yr BP, assuming the reliability of our basal AMS radiocarbon age on charcoal (UCIAMS # 89213). However, our proxy data from Unit 1 sediments (see Discussion) suggest the possibility that old organic material was reworked into presumably younger sediments, and thus age constraints and calculated sedimentation rates prior to 16,800 yr BP may be erroneous. Subsequently, sedimentation rates increased to 0.010 cm/yr from 16,800 yr BP to 12,700 yr BP. At 12,700 yr BP, the sedimentation rate again increased to 0.031 cm/yr until 12,000 yr BP. Thereafter (between 12,000 yr BP and 9,400 yr BP) sedimentation rates were lower, ~0.01 cm/yr. At 9,400 yr BP, the sedimentation rate greatly increased to 0.225 cm/yr, a rate that was maintained until 9,100 yr BP. During this interval sediment accumulated more rapidly at Harding Lake than any other time during the late Quaternary (see results and discussion for Lithologic Unit 3). Subsequently, sedimentation rates were lower from 9,100 yr BP to 109 yr BP, with values between ~0.015 and ~0.040 cm/yr. Sedimentation rates for the upper 10 cm were calculated from ^{210}Pb ages and increase from 0.03 cm/yr to 0.2 cm/yr from 109 to −60 yr BP (2010 AD), respectively.

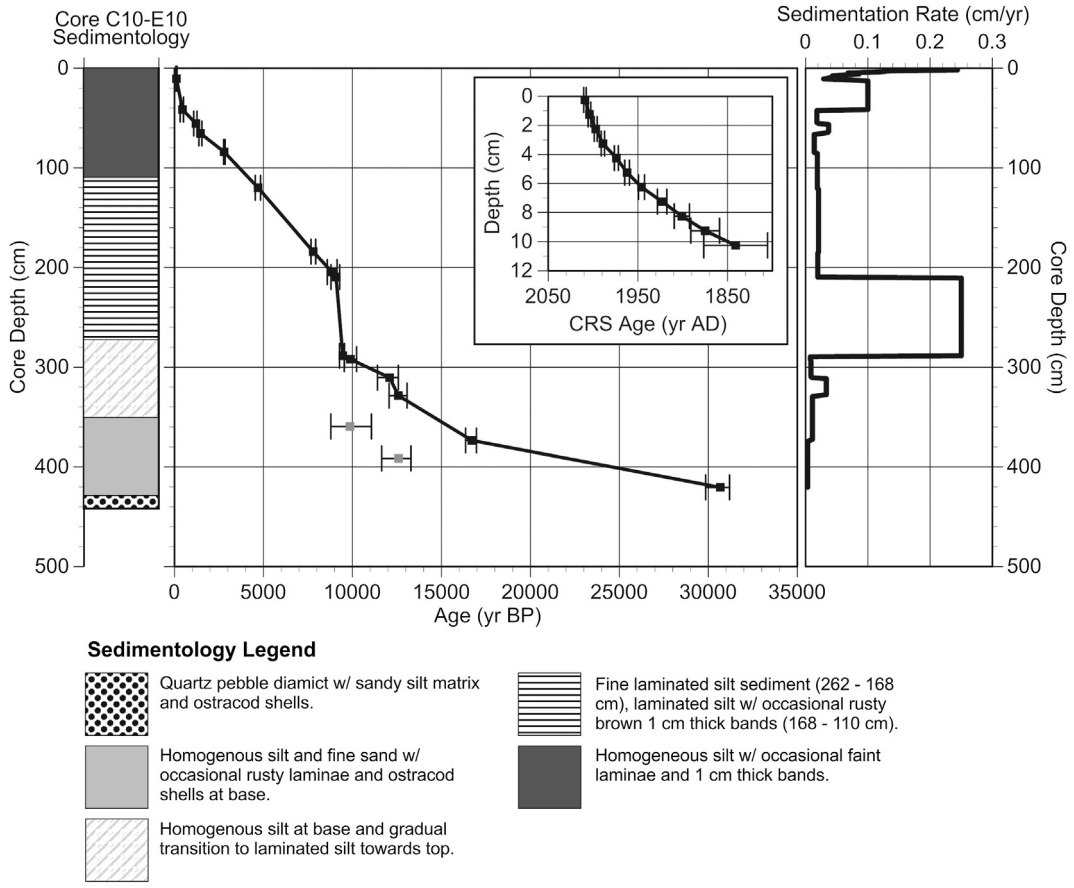

Fig. 4. Composite core sedimentology and age-depth model developed from the AMS radiocarbon and ^{210}Pb profile generated with the CLAM code for R software (Blaauw, 2010) with linear sedimentation rates (cm/yr). Gray squares indicate stratigraphically reversed dates that were rejected from the age model due to extremely small carbon yields and presumed modern carbon contamination.

4.2. Composite sediment core lithologic units

Our paleoenvironmental interpretation of the Harding Lake record is based on lithologic units defined using the sediment physical and geochemical data. We identified 4 lithologic units based primarily on variations in organic matter (wt %), biogenic silica (wt %), and magnetic susceptibility (Table 2; Figs. 5, 6) as well as 4 pollen zones (Table 3; Fig. 7). The lithologic unit boundaries do not correspond to the changes in sedimentation rate (Fig. 4); however, this is not expected given these calculations are based on a linear interpolation between the radiocarbon and ^{210}Pb ages. In addition, the lithologic and pollen boundaries are broadly similar, but do not correspond exactly.

4.3. Lithologic Unit 1

Unit 1 extends from the base of the composite core (422 cm) to 352 cm depth and spans the period 30,700–15,700 yr BP. The basal 7 cm (422–416 cm) consist of a dusky brown (5YR 2/2), quartz pebble diamicton with abundant ostracod shells and a sandy silt matrix. The upper portion (416–352 cm) gradually transitions to pale brown (5YR 5/2) to pale yellowish brown (10YR 6/2), homogenous silt and fine sand with occasional rusty laminae and ostracod shells at the base. Smear-slide analysis of several samples shows very few diatom frustules or sponge spicules and a large proportion of mineral matter. Diatoms in this unit are often fragmented and appear to have been partially dissolved. Unit 1 sediments are characterized by relatively coarse grain size (silt to fine sand), along with high and variable magnetic susceptibility (19 ± 4 SI) and dry bulk density values (1.1 ± 0.1 g/cm^3). Organic matter (4 ± 1%) and biogenic silica (1 ± 0.3%) contents are very low while titanium (6300 ± 1300 cps) concentrations are relatively high. The organic matter and biogenic silica content in Unit 1 gradually increases and peaks at 383 cm and 380 cm, respectively, and subsequently decreases gradually until the Unit 2 boundary (Fig. 5). Organic matter δ^{13}C values (−27 ± 0.7‰) are high and exhibit considerable variability. C/N ratios are on average low (10 ± 0.9) during this interval. Pollen zone 1 spans the entirety of lithologic Unit 1 and is predominated by herb taxa including Cyperaceae, Poaceae, and *Artemisia* (Fig. 7). *Salix* and *Betula* are a minor component of the pollen assemblage. Pre-Quaternary pollen and spores are present in low amounts, indicating possible reworking of older sediments into the lake basin. The aquatic taxa *Myriophyllum* and *Pediastrum* (Fig. 7) are also consistently present.

Table 2
Harding Lake lithologic units, transitions inferred based on changes in organic matter (LOI 550 by wt. %), biogenic silica (wt. %), and magnetic susceptibility (SI).

Lithologic unit	Core depth (cm)	Age range (yr BP)
4	193–0	8,700–2010 AD
3	262–193	9,400–8,700
2	352–262	15,700–9,400
1	422–352	30,700–15,700

4.4. Lithologic Unit 2

Unit 2 extends from 352 cm to 262 cm depth and spans the period 15,700–9,400 yr BP. The contact with Unit 1 sediments is

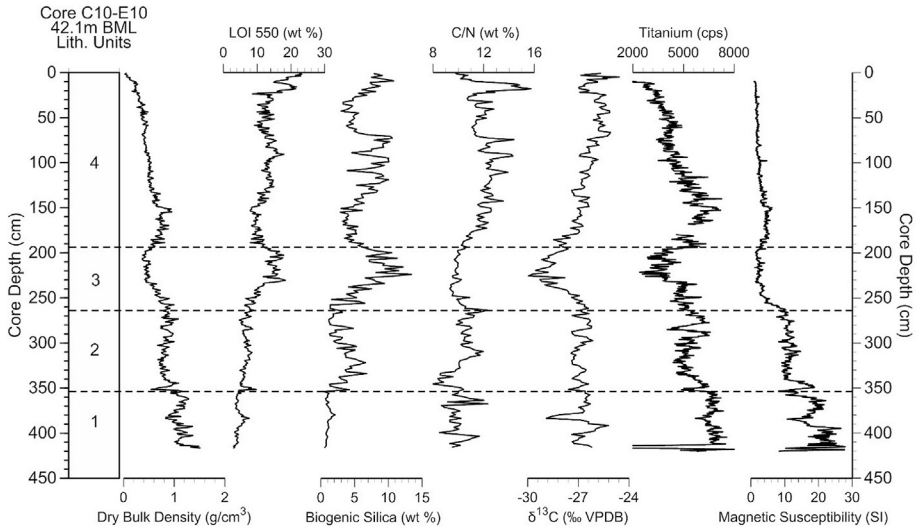

Fig. 5. Harding Lake composite core proxy data plotted against depth. Lithologic units are defined primarily by variability in organic matter, biogenic silica, and magnetic susceptibility.

gradual, and the lower portion (352–272 cm) consists of dusky brown (5YR 2/2) to pale brown (5YR 5/2) silt, homogenous at the base and increasingly laminated towards 261 cm. The upper portion (272–262 cm) consists of dark yellowish brown (10YR 4/2), dusky yellowish brown (10YR 2/2), and dusky brown (5YR 2/2) laminated silt. Smear slide analysis shows a higher proportion and increased diversity in diatom frustules and sponge spicules compared to Unit 1. Unit 2 sediments are characterized by decreasing grain size (silt), along with intermediate magnetic susceptibility (10 ± 3 SI) and titanium (5400 ± 500 cps) values compared to Units 1 and 3–4. Dry bulk density (0.9 ± 0.9 g/cm^3) abruptly decreases then increases at the base of Unit 2, and subsequently decreases again up core (Fig. 5). Organic matter values (7 ± 1%) are higher compared to Unit 1 and increase at the base of Unit 2 then rapidly decrease (Fig. 5). The organic matter content gradually increases up core with minor variability to 12,300 yr BP then steadily decreases to 9400 yr BP, with minor variability at the top of Unit 2. Biogenic silica values (3 ± 1%) are also higher than Unit 1, and gradually increase and peak between 13,900 and 12,700 yr BP then gradually decrease to 9400 yr BP, with some variability during this interval (Fig. 5). Organic matter δ^{13}C values (−27 ± 0.4‰) are similar to Unit 1 and fluctuate substantially. C/N ratios (10 ± 1) initially decline and gradually increase up section through Unit 2 (Fig. 5). Pollen zone 1 persists until 341 cm (14,600 yr BP), and thereafter pollen zone 2 begins and is marked by a fourfold increase in pollen concentration (not shown). It is characterized by the *Betula* rise, a regional feature, and subsequent high *Betula* values (>50%). *Salix* is a minor component (<10%) of the pollen assemblage during this interval. There is a corresponding decline in herb taxa (Fig. 7), but Cyperaceae values remain moderately high, possibly reflecting local vegetation associated with the lake basin.

4.5. Lithologic Unit 3

Unit 3 extends from 262 cm to 193 cm and spans the period 9,400–8,700 yr BP. Sediments consist of dark yellowish brown (10YR 4/2), dusky yellowish brown (10YR 2/2), and dusky brown (5YR 2/2) laminated silt. The contact between Unit 2 sediments is gradational. Smear slide analysis shows the highest proportion and diversity in diatom frustules and sponge spicules for the entire record. Unit 3 sediments are characterized by silty sediments with

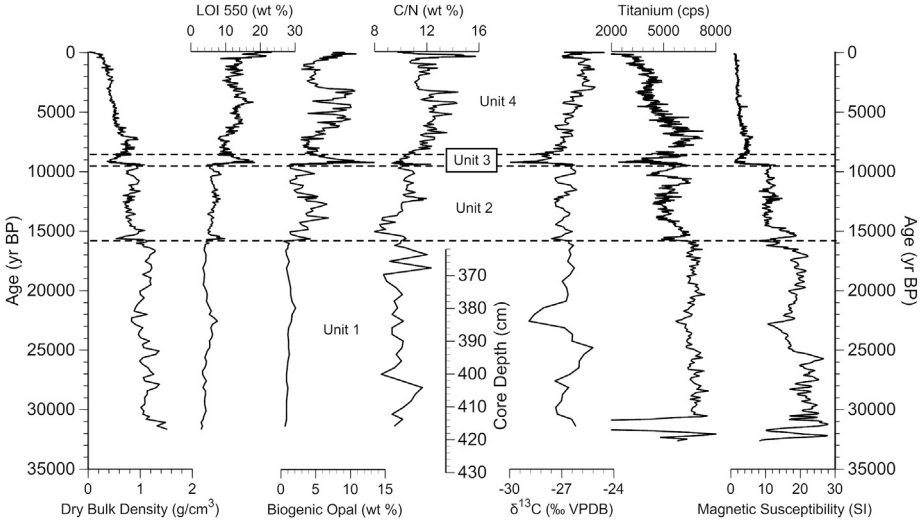

Fig. 6. Harding Lake composite core proxy data plotted against age in yr BP. Data also plotted against core depth (cm) for Unit 1 sediments spanning the Last Glacial Maximum.

Table 3
Harding Lake pollen zones.

Pollen zone	Core depth (cm)	Age range (yr BP)	Dominant taxa
3	200–0	9,100–present	*Betula*, *Alnus*, and *Picea*
2	341–200	14,600–9,100	*Betula*
1	422–341	30,700–14,600	Herb

an abrupt and sustained increase in organic matter (13 ± 3%) and biogenic silica (7 ± 3%) concentration, and a corresponding decrease in dry bulk density (0.6 ± 0.1 g/cm^3) (Fig. 5). Biogenic silica content peaks and attains the highest value (13%) for the entire Holocene at 9,200 yr BP. In addition, the organic matter content peaks (18%) at 9,200 yr BP, reaching a level that matches late Holocene values. Magnetic susceptibility (3 ± 2 SI), titanium (4300 ± 800 cps), and dry bulk density (0.6 ± 0.1 g/cc) are much lower in comparison to Units 1 and 2 (Fig. 5). Organic matter $\delta^{13}C$ values (−28 ± 0.2‰) abruptly decrease and are the most negative for the entire record. C/N ratios (10 ± 0.4) are generally low, stable, and comparable to Unit 1 and 2 sediments, although with much less variability (Fig. 5). We suggest the abrupt and sustained decrease in $\delta^{13}C$ and low C/N values is a result of increased aquatic productivity and loading of dissolved relatively depleted $\delta^{13}C$ carbon to the lake from the watershed. This interval overlaps with the time of highest sedimentation (0.225 cm/yr) throughout the entire record and indicates a major change within the lake and the surrounding landscape. Given that sedimentation rates increase through this interval and titanium values decrease, likely caused by dilution from organic matter, we interpret the increase in organic matter and biogenic silica content as a result of increased in-lake productivity. The main components of the pollen spectra retain the features of pollen zone 2.

4.6. Lithologic Unit 4

Unit 4 extends from 193 cm to the top of the composite core (0 cm) and spans the period 8,700 yr BP to 2010 AD. The contact between Unit 3 sediments is gradational. The lower portion (193–168 cm) consists of consists of dark yellowish brown (10YR 4/2), dusky yellowish brown (10YR 2/2), and dusky brown (5YR 2/2) laminated silt. The middle portion (168–110 cm) consists of dark yellowish brown (10YR 4/2) laminated silt with occasional dusky brown (5YR 2/2) 1 cm thick bands. The upper portion consists of dark yellowish brown (10YR 4/2) to brownish black (5YR 2/1) homogenous silt with occasional faint laminae and banding. Smear slide analysis shows a high proportion and diversity in diatom frustules and sponge spicules throughout this interval. Unit 4 sediments are characterized by fine-grained sediments (silt), along with moderately high and variable organic matter (13 ± 3%) and biogenic silica (6 ± 2%) concentrations with slightly different trends (Fig. 5). Biogenic silica gradually increases up section and peaks at values >10% between 120 and 70 cm (5,500 and 3,100 yr BP) with substantial variability (Fig. 5). Generally low values of biogenic silica are found between 70 and ~26 cm (3,100–600 yr BP) with a generally rising trend up core to ~10% near the core top (Fig. 5). In contrast, organic matter steadily increases and peaks at 18% at a depth of 91 cm (4,100 yr BP), exhibiting minimal variability. Above this, organic matter decreases up core with values generally <15% until 23 cm (450 yr BP) (Fig. 5). Organic matter values increase to the highest levels of the entire record (23%) near the core top (over last 450 yr) with substantial variability. Organic matter $\delta^{13}C$ (−26 ± 0.7‰) gradually increases up core from −28‰ and approach values of −25‰ between 70 and ~25 cm (3,100–600 yr BP) and near the core top at 5 cm (Fig. 5). C/N ratios (12 ± 1) gradually increase up section from the base of Unit 4 to high values (~14) with substantial variability (~2) from 110 to 74 cm (5,100–3,300 yr BP) (Fig. 5). The highest C/N ratios are found near the core top between 19 and 13 cm and peak at values >15. Magnetic susceptibility (3 ± 1 SI), titanium (4800 ± 1000 cps), and dry bulk density (0.5 ± 0.1 g/cm^3) values steadily increase and peak by 7,100 yr BP and gradually decrease up section to the core top (Fig. 5). Sedimentation rates (~0.015–~0.04 cm/yr) were generally stable and low throughout Unit 4 until ~109 yr BP and thereafter gradually increase towards the core top to 0.2 cm/yr,

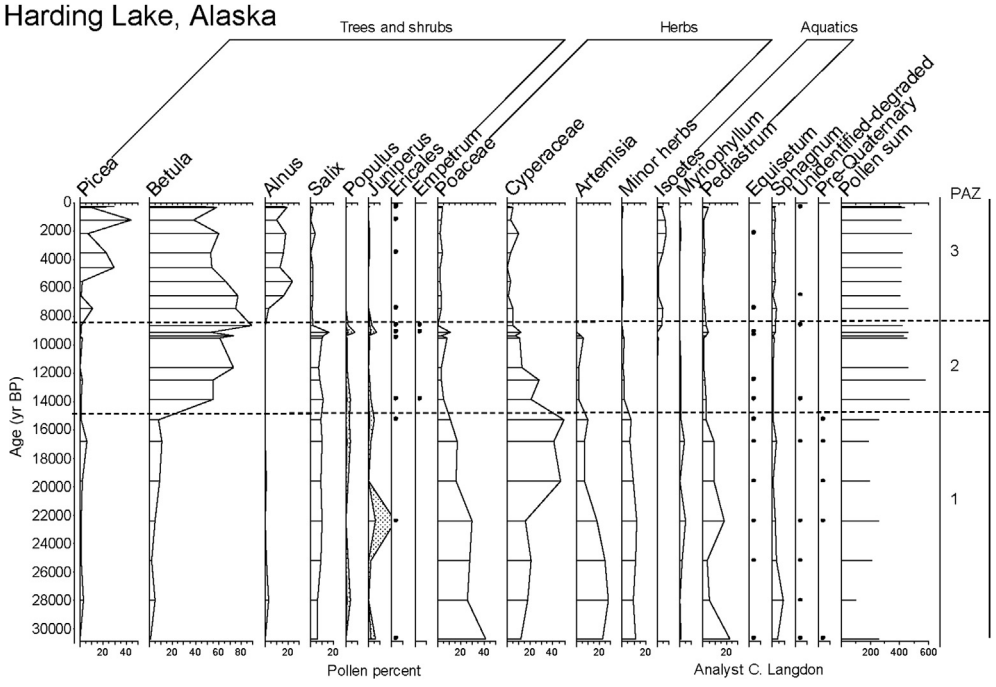

Fig. 7. Harding Lake frequencies (percentages) of major pollen and spore taxa plotted against age in yr BP.

indicating stability in landscape and climatic conditions. Pollen zone 3 begins about 9,100 yr BP and covers the uppermost part of the record. High *Betula* (>75%) pollen predominates, and values of *Picea* and *Alnus* increase between 8,600 and 7,500 yr BP. *Isoetes* predominates the aquatic taxa and *Myriophyllum* is absent.

4.7. Core F-10 sediments

Core F-10 was recovered in 7.1 m water depth, is 32.5 cm in length, and spans the sediment–water interface (Fig. 8). The upper 8 cm consist of dark yellowish brown (10 YR 4/2) to pale yellowish brown (10YR 6/2) homogenous silt to fine sand. The remainder of the sediment between 8 and 32.5 cm consists of grayish brown (5YR 3/2) homogenous silt to fine sand interrupted by grayish brown sand layers. The medium to coarse grained sand layers are from 13 to 15.5 cm and 20 to 20.5 cm, with erosive contacts and load structures immediately below the sand. Smear slide analysis of select samples shows diatom frustules in the upper portion (0–13 cm) while the basal sediments consist entirely of mineral sediment with no diatoms. Dry bulk density (1 ± 0.3 g/cm^3) is generally high throughout and gradually decreases up core. Organic matter ($7 \pm 3\%$) is low at the core bottom and generally increases towards the core top. Magnetic susceptibility (49 ± 82 SI) is very high at the core bottom and gradually decreases towards the top. No terrestrial macrofossils were found for radiocarbon dating of core F-10.

4.8. Core A-12 sediments

Core A-12 was recovered in 10.75 m water depth, is 55 cm in length, and starts 20 cm below the sediment–water interface (Fig. 8). The upper portion (20–74 cm) consists of dark yellowish brown (10YR 4/2) homogenous to faintly banded silt to find sand and the basal 1 cm (74–75 cm) consists of medium sand. Smear slide analysis of select samples shows diatom frustules in the upper portion (20–74 cm) of the sediments. Dry bulk density (0.6 ± 0.2 g/cm^3) values gradually decrease up core while organic matter ($10 \pm 2\%$) values generally increase towards the core top. Magnetic susceptibility (14 ± 13 SI) is very high at the core bottom and gradually decreases towards the top. Radiocarbon analysis of a seed at 73–74 cm constrains the onset of lacustrine sedimentation at the core site (11.48 m below modern level; BML) to 15,050 yr BP (Table 1; 13,910–16,520 yr BP error range). No other terrestrial macrofossils were found in core A-12 for radiocarbon dating.

4.9. Core E-12 sediments

Core E-12 was recovered in 15.91 m water depth, is 108 cm in length, and starts 20 cm below the sediment–water interface (Fig. 8). The upper portion (20–110 cm) consists of moderate yellowish brown (10YR 5/4) to dark yellowish brown (10YR 4/2) homogenous to faintly banded silt. The middle portion (110–118 cm) consists of disturbed, moderate yellowish brown (10YR 5/4) to dark yellowish brown (10YR 4/2) silt to fine sand sediment with a clear erosional unconformity. The basal sediments (118–128 cm) consist of dark yellowish brown (10YR 4/2) silt and fine to medium sand with organic rich layers from 118 to 123 cm. Smear slide analysis of select samples shows diatom frustules in the upper 90 cm (20–110 cm) while the basal sediments largely consist of mineral matter. Dry bulk density (0.8 ± 0.3 g/cm^3) values generally decrease up core, aside from the unconformity interval resulting from erosion and re-working (Fig. 8). Organic matter ($8 \pm 2\%$) values generally increase and magnetic susceptibility (57 ± 40 SI) values generally decrease towards the core top, again aside from the unconformity interval (Fig. 8). Radiocarbon analysis was conducted on three samples from core E-12 (Table 1). A sample of wood from 120 to 121 cm constrains the onset of lacustrine sedimentation at the core site (17.11 m BML) to 14,020 yr BP (13,870–14,170 yr BP error range). An additional sample of wood from 118 to 119 cm has a median age of 13,720 yr BP (13,110–14,830 yr BP error range) and provides further evidence of the initial major rise in lake level. The median ages of these samples are in stratigraphic order; however the calibrated error ranges overlap. A sample of wood from 93 to 94 cm, located stratigraphically above the erosional unconformity in the E-12 core, constrains the subsequent rise in lake level (16.84 m BML) to before 9,660 yr BP (9,470–10,120 yr BP error range).

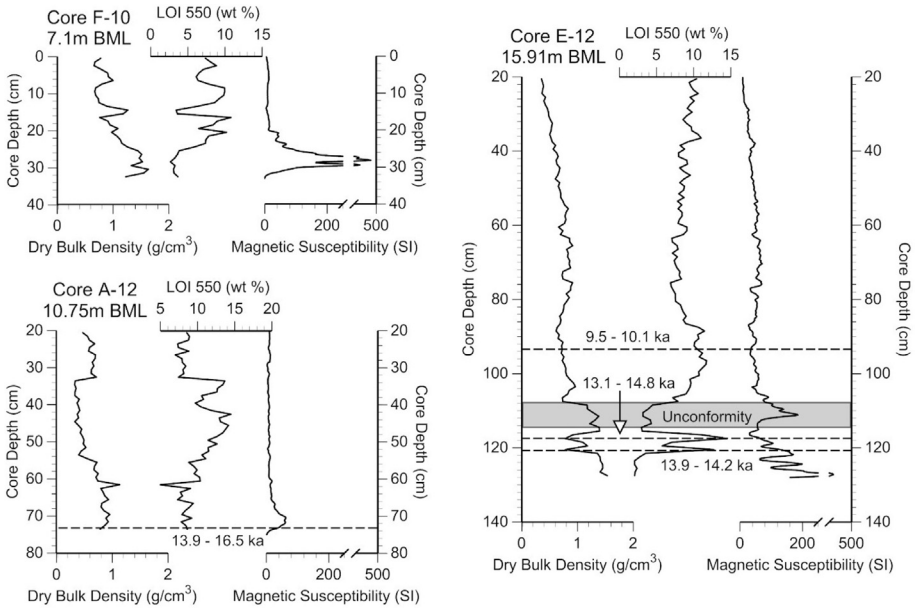

Fig. 8. Harding Lake cores F-10, A-12, and E-12 proxy data plotted versus depth. Dashed lines indicate radiocarbon samples, reported as the calibrated 2 sigma error range in thousands of years (ka) before present.

5. Discussion

The specific climatic controls on lake level at multi-centennial to millennial timescales at Harding Lake are poorly understood, though must be related to changes in regional effective moisture (precipitation minus evaporation). Sediment proxies from Harding Lake show that variability in organic matter content and magnetic susceptibility are coeval with many regional hydroclimate transitions evidenced from other paleoproxy datasets. Scatterplot analysis of organic matter content and magnetic susceptibility (Fig. 9A) demonstrates clustering of the lithologic units into distinct groups. Unit 1 (30,700–15,700 yr BP) sediments, characterized by the lowest organic matter content and highest magnetic susceptibility during the entire record, correspond to the interval when most small, shallow lakes in central Alaska were dry (eg. Ager, 1983; Abbott et al., 2000; Bigelow and Edwards, 2001; Carlson and Finney, 2004; Wooller et al., 2012). Unit 2 (15,700–9,400 yr BP) sediments, characterized by intermediate organic matter content and magnetic susceptibility, parallel the initial formation of lacustrine sediment in many lakes in central Alaska, indicating rising and fluctuating water levels (eg. Abbott et al., 2000). In contrast, Unit 3 and 4 (9,400 yr BP to present) sediments, characterized by high organic matter content and low magnetic susceptibility, were deposited during the Holocene when regional lake levels were rising and near overflow levels (eg. Bigelow, 1997; Abbott et al., 2000; Bigelow and Edwards, 2001; Carlson and Finney, 2004; Finney et al., 2012; Wooller et al., 2012). However, variability in organic matter content and magnetic susceptibility may also in part reflect changes in soil stabilization within Harding Lake's watershed associated with vegetation shifts. For example, Hu et al. (1993) suggested that shrub tundra conditions between 12,000 and 10,500 ^{14}C yr BP (~13,900 to ~12,500 yr BP) at Wien Lake (central Alaska) were accompanied by intensive soil erosion, inferred from high allogenic metal and low sediment organic content. The relatively sparse vegetative cover during this time likely promoted weathering and erosion of bare mineral soils in the surrounding watershed. The subsequent transition to shrub and boreal forest beginning at 10,500 ^{14}C yr BP (~12,500 yr BP) was marked by lower allogenic metal and higher sediment organic content, which Hu et al. (1993) attributed to the buildup of humic compounds and stabilization of watershed soils. Additional lake studies from northwestern (Hu et al., 1996) and southwestern (Hu et al., 2001) Alaska revealed similar vegetation-landscape development associated with the tundra to boreal forest transition during the late Pleistocene and early Holocene.

Scatterplot analysis of organic matter content and magnetic susceptibility from the upper portion (10–20 cm) of cores collected along a depth transect (Fig. 9B) confirms the aforementioned relationship and provides semi-quantitative constraints on lake-levels. For example, core top sediments from deep water cores B-10 and C-10 recovered from 38.05 to 42.1 m BML, and characterized by high organic matter content and low magnetic susceptibility (Fig. 9B), indicate that modern deep water sediments are most similar to middle to late-Holocene sediments from the composite core. In addition, surface sediments from shallow water cores F-10, A-12, and E-12 recovered from 7.1, 10.75, and 15.91 m BML and characterized by intermediate organic matter content and magnetic susceptibility (Fig. 9B), indicate that modern shallow to intermediate water sediments are most similar to Lateglacial sediments. Although a minor component of the down-core variability in organic matter content and magnetic susceptibility may be related to vegetation-landscape development (described above), the substantial variation in sediment properties along a water depth transect in the modern system suggests that vegetation-landscape changes were likely a small influence. We therefore assert that water depth is the dominant control at multi-centennial to millennial timescales on organic matter content and magnetic susceptibility. The lack of fine sediment deposition in water levels shallower than 7 m indicates that wave base erosion occurs to this depth in the modern lake.

Pompeani et al. (2012) used scatterplot analysis for Rantin Lake sediments in the Yukon (Canada) to distinguish deep versus shallow water sediment properties. In addition, Edwards et al. (2000) used a similar model in their investigation of Birch Lake using surface sediments along a water depth transect, where trends in sediment properties (aquatic pollen proportion along with organic matter and magnetic susceptibility) reflected similar lake-level changes as determined from transect based lake-level

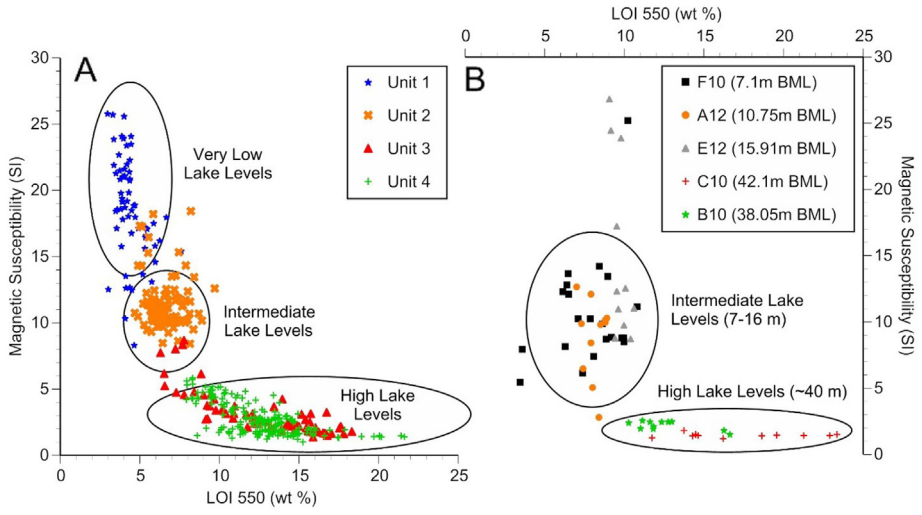

Fig. 9. A) Scatterplot of organic matter content (LOI 550) versus magnetic susceptibility (SI) for the Harding Lake composite core plotted by lithologic unit and B) surface sediments from core F-10, (7.1 m BML), A-12 (10.75 m BML), E-12 (15.91 m BML), B-10 (38.05 m BML), and C-10 (42.1 m BML). We utilize this conceptual model (i.e. changes in organic matter content and magnetic susceptibility) to interpret relative lake-level changes. Shallow water sediments are characterized by high magnetic susceptibility and low organic matter. Intermediate water depths are characterized by moderate magnetic susceptibility and organic matter content (eg. Unit 2 corresponds to core F-10, A-12, and E-12 sediment properties from 7 to 16 m water depths). Deep water sediments are characterized by low magnetic susceptibility and high organic matter content (eg. Unit 3-4 sediments correspond to core B-10 and C-10 sediment properties from 38 to 42 m water depths).

reconstructions (Abbott et al., 2000). Edwards et al. (2000) also collected surface sediment samples from modern lakes in interior Alaska and used pollen analysis to investigate the relationship between aquatic taxa and water depth. Notably, a higher diversity of aquatic taxa was found at shallower (<5 m) water depths, with little to no aquatic taxa found at depths >20 m. Core transect data also demonstrate that a substantial lake-level rise and fluctuating water levels occurred during the Lateglacial period. The basal radiocarbon age from core A-12 suggests the initial rise in lake level to <11.5 m BML occurred ~13,900–16,500 yr BP. This sample (UCIAMS # 131490) has large analytical uncertainty, and the basal radiocarbon ages from core E-12 better constrain the lake level rise (to <17.1 m BML) at ~14,000 yr BP. The erosional unconformity in core E-12 above the basal sediments (Fig. 8) represents a period of non-deposition at this core site or erosion of previously deposited sediments during a time of lower or fluctuating lake levels after ~14,000 yr BP. The subsequent rise in lake-level to <16.8 m BML is constrained by the uppermost radiocarbon age of 9,660 yr BP from core E-12 in fine-grained lacustrine sediment located above the erosional unconformity. There is no evidence that lake level dropped below the E-12 core site after this time. Accordingly, we combine the organic matter to magnetic susceptibility conceptual model with core-transect data to infer semi-quantitative changes in lake-level at Harding Lake (Fig. 10A) and compare these results with paleoclimate datasets from eastern Beringia. We do not account for the depth of wave base erosion in our lake level curve (Fig. 10A) and therefore our lake level constraints are semi-quantitative. However, we surmise the wave base erosion depth was of a lower magnitude during the period of rapid lake level change (during the Lateglacial) when the lake surface area was presumably smaller.

5.1. Pre-Last Glacial Maximum (>30,700 yr BP)

The presence of coarse sediments (pebble diamicton), low concentrations of organic matter and biogenic silica, and high and variable magnetic susceptibility, titanium, and dry bulk density indicate the basal 7 cm of Unit 1 are the lake bottom substrate (Fig. 6). The lack of finer grained lacustrine sediments further indicates that prior to 30,700 yr BP the lake was either seasonally desiccated or dry for a long period of time, with any previously deposited sediment removed by deflation or fluvial reworking. The occurrence of these coarse sediments is consistent with the conclusions of Blackwell (1965) that Harding Lake was formed by aggradation of Tanana River through deposition of braided stream sediments and subsequent damming of the proto Salcha River draining from the north. Blackwell (1965) suggested the lake basin formed during the Delta Glaciation (penultimate), which has recently been dated by cosmogenic exposure ages to late Marine Isotope Stage (MIS) 4 or early MIS3, approximately 60,000–50,000 yr BP (Kaufman et al., 2011). If this age assignment is correct, the absence of lacustrine sediments dating to this time indicates generally unstable and variable climatic conditions with significant

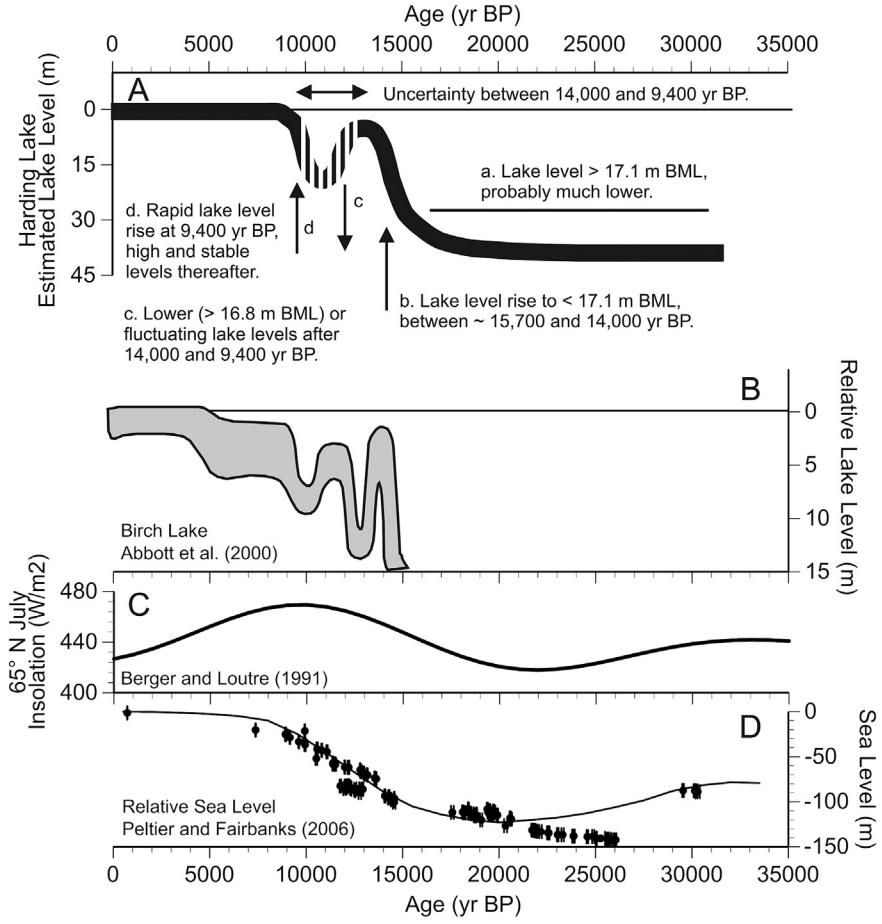

Fig. 10. A) Lake-level curve for Harding Lake inferred from core-transect data and sediment physical and geochemical properties. The dashed line between 14,000 and 9,400 yr BP represents uncertainty in the reconstruction due to lower (>16.8 m below modern level; BML) or fluctuating lake-levels during this time. B) Comparison with a lake-level reconstruction for Birch Lake, Alaska determined from seismic profiles and core transects (Abbott et al., 2000). C) July insolation (watts/m^2) for 65° North (Berger and Loutre, 1991). D) Relative sea level data (Peltier and Fairbanks, 2006) and the ice-equivalent eustatic sea level history (smooth black line) (Waelbroeck et al., 2002).

aridity during MIS3 in central Alaska, which may have caused multiple transgression/regression events that eroded sediment from the basin. Alternatively, previously deposited sediments may have been subsequently removed via fluvial erosion or deflation when lake levels were lower.

The existence of loess deposits stratigraphically above palaeosols dating to 32,000–30,000 ^{14}C yr BP (36,500–34,700 yr BP) at Halfway House, Gold Hill, and Birch Hill near Fairbanks (Muhs et al., 2003) indicates this was a time of extremely arid and windy conditions. Pollen data from Isabella Basin demonstrate high percentages of Cyperaceae and *Artemisia* and low percentages of *Alnus* and *Picea* after ~32,000 ^{14}C yr BP until the Holocene (Matthews, 1974). Matthews (1974) interpreted these data to represent arctic climatic conditions in central Alaska, similar to that of the present day tundra in northern Alaska. Pollen and grain size data are available from a previous investigation of Harding Lake sediments (Nakao and Ager, 1985). While relatively coarse sediments (sand to granule) are recorded prior to 26,500 ± 460 ^{14}C yr BP (31,000 yr BP), pollen data are interpreted to show a vegetational mosaic characterized by *Picea*, *Betula*, *Ericales*, Cyperaceae and *Sphagnum*. Nakao and Ager (1985) suggest these proxies represent middle Wisconsian Interstadial conditions and a cool, wet climate; however, the use of bulk sediment radiocarbon dating, the presence of an age reversal in this interval, and the use of conventional drilling techniques to recover sediments may compromise their interpretation.

5.2. The global Last Glacial Maximum (30,700–15,700 yr BP)

The portion of Unit 1 stratigraphically above the coarse basal sediment is characterized by decreasing grain size (silt to fine sand) with high and variable dry bulk density and generally constant titanium content (Fig. 6), and an extremely low sedimentation rate (Fig. 4), assuming reliability of our basal radiocarbon age on fine (<250 μm) charcoal. Sediments are homogenous with occasional rusty banding, and there is no evidence of unconformities (eg. mud cracks, erosional surfaces, etc.) that would indicate discontinuous sedimentation. We suggest these sediments were deposited in a nearly perennially frozen, shallow lake with a very short ice free summer season. Low organic matter and biogenic silica concentration imply that terrestrial vegetation was scarce in the vicinity and that in-lake productivity levels were low, due to cold and potentially turbid waters. High magnetic susceptibility and low organic matter content, combined with the absence of glacial age sediments in cores from shallower water depths, suggest very shallow lake levels (Fig. 10A). The general absence of terrestrial macrofossils in Unit 1 sediments further indicate the surrounding landscape had sparse vegetation. The predominance of herb taxa (Cyperaceae, Poaceae, and *Artemisia*) during the LGM (Fig. 7) suggests a tundra environment with cold and dry conditions relative to today. The aquatic taxa *Myriophyllum* and *Pediastrum* (Fig. 7) are consistently present and together indicate shallow water conditions (eg. Edwards et al., 2000), which is coherent with low organic matter content and high magnetic susceptibility values in Unit 1 and the absence of LGM age sediments in shallow water cores. The high magnetic susceptibility and titanium values resulted from a high concentration of fine-grained clastic-rich sediments, which likely originated from wind-blown loess or intensive erosion of watershed soils. Age control during this interval rests on the basal charcoal sample at 412.5 cm (UCIAMS # 89213) and a linear interpolation to the next age at 362.5 cm. While the analytical uncertainty of the basal sample is generally low considering its age (Table 1), the question remains whether the organic material formed and subsequently deposited contemporaneously with the enclosing sediments. We believe the charcoal sample was formed and deposited simultaneously with the surrounding sediments because charcoal is extremely friable and easily disintegrates with minimal physical erosion. Given that Unit 1 sediments above the coarse basal gravel lack any convincing evidence of unconformities (explained above), we infer these sediments represent temporally continuous sedimentation from ~30,700 to 15,700 yr BP. Alternatively, it is possible that the basal charcoal material could be reworked from older sediments, and therefore the timing of initiation of lacustrine sedimentation may be younger than its reported radiocarbon age. This scenario is consistent with the presence of only tundra type vegetation in Unit 1 sediments, which typify LGM conditions in interior Alaska, but continuous records dating the onset of tundra vegetation are lacking.

The proxy data from Harding Lake are consistent with evidence from central Alaska showing extremely arid conditions during the LGM. A revised model for loess deposition indicates that loess production and windiness increased during the LGM in central Alaska while accumulation decreased because of a lack of vegetative cover (Muhs et al., 2003). AMS radiocarbon and ^{10}Be dates from loess deposits near Fairbanks (Halfway House, Gold Hill, and Birch Hills; Muhs et al., 2003) also suggest minimal loess deposition occurred during the global LGM because of the presence of sparse herb-tundra vegetation and minimal ground surface roughness. Nakao and Ager (1985) report the predominance of herb taxa from Harding Lake and suggest that climate was extremely cold and dry between 26,500 ± 460 and 13,690 ± 500 ^{14}C yr BP (31,000–16,500 yr BP). An unconformity in the sedimentary record from Burial Lake in northwest Alaska indicates a significant drop in lake level and a hiatus in deposition between 34,800 and 23,200 yr BP (Abbott et al., 2010). Core transect data from Birch Lake in the Tanana Valley indicate lake levels were 18 m lower prior to 15,000 yr BP (Fig. 10B; Abbott et al., 2000). Evidence from elsewhere in the unglaciated interior of Alaska show that most small lakes were dry prior to the Lateglacial (15,000 yr BP) (eg. Ager, 1983; Bigelow, 1997; Bigelow and Edwards, 2001; Carlson and Finney, 2004; Wooller et al., 2012).

Collectively, these proxy records demonstrate an extremely dry climate in central Alaska during the global LGM that is, in part, attributed to changes in atmospheric circulation and exposure of the Bering Land Bridge. In climate model simulations for the LGM (18,000 yr BP), the winter jet-stream is split into a northern and southern component by the high-altitude dome of the Laurentide Ice Sheet (COHMAP Members, 1988). Simultaneously, an anticyclonic circulation ('glacial anti-cyclone') developed at the surface with enhanced easterly winds at the southern margin and southerly winds at the western margin of the ice sheet (Bartlein et al., 1991). The climatic effects of changing circulation were spatially variable and complicated, but likely produced windy and dry conditions downwind of the Laurentide Ice Sheet. Eustatic sea level lowering of −120 m (Fig. 10D; Peltier and Fairbanks, 2006) resulted in exposure of the Bering and Chukchi continental shelves (Hopkins, 1982), forming the land bridge and increasing the transport distance of moisture from the North Pacific Ocean and Bering Sea (eg. Briner and Kaufman, 2000) to interior Alaska. The substantial increase in distance from oceanic moisture sources caused the climate of interior regions to become even more continental and dry.

Several recently published glacial records using cosmogenic exposure dates from moraines further document climatic conditions during the LGM. Evidence from Ramshorn Creek valley in the Yukon-Tanana Uplands shows the LGM maxima (Salcha moraine) occurred between 23,000 and 21,000 yr BP during the northern hemisphere summer insolation minima (Fig. 10C), while a recessional moraine located ~3.5 km up-valley (Ramshorn moraine) dates to between 19,000 and 18,000 yr BP (Briner et al., 2005). A cosmogenic exposure chronology from Fish Lake valley in the

northeast Alaska Range shows the LGM maxima may have occurred by 22,400 ± 600 yr BP (Young et al., 2009); however this age is based on only one date. Young et al. (2009) report a clustering of younger ages that suggest the Fish Lake glacier remained near the LGM maxima until ~16,500 yr BP. Evidence from the Delta River valley, the type section for late Pleistocene (Wisconsinan) glaciation in the northeast Alaska Range, dates the Donnelly moraine to 17,300 ± 600 yr BP (Matmon et al., 2010). These cosmogenic exposure chronologies suggest that regional glaciers persisted at or near their LGM maxima until near the Lateglacial transition, implying that climatic conditions remained favorable (likely colder) for positive glacier mass balance until 17,000–16,000 yr BP. Glacier mass balance is controlled by both temperature and precipitation conditions, and while the LGM climate of interior Alaska is considered extremely dry (Hopkins, 1982), glacial maxima during the LGM likely resulted from colder temperatures. Therefore, the timing of alpine glacier retreat during the Lateglacial (beginning around ~16,000–17,000 yr BP) likely indicates the initiation of warmer conditions.

Although our age control is limited during the LGM, proxy data from Harding Lake permit critical testing of an LGM (21,000 yr BP) climate model simulation that indicate annual temperatures up to 4 °C warmer than present in central Alaska (Otto-Bliesner et al., 2006). Likewise, the conclusions from Otto-Bliesner et al. (2006) are broadly supported by a pollen based LGM climate reconstruction (Bartlein et al., 2011) that relies on several pollen records constrained with bulk sediment radiocarbon dates. The anomalously warmer temperatures are hypothetically explained by the aforementioned changes in atmospheric circulation associated with the increasing size and altitude of the Laurentide Ice Sheet (eg. COHMAP Members, 1988). Otto-Bliesner et al. (2006) suggest the strong pressure gradient between the high pressure cell over the Laurentide Ice Sheet centered near Hudson Bay and a low pressure region in the North Pacific (Aleutian low) resulted in stronger southerly surface winds on the western margin of the ice sheet. Model simulations indicate the enhanced winds produced poleward advection of warmer air into Alaska, especially during winter (COHMAP Members, 1988). Although our age control is limited, evidence of very low aquatic (biogenic silica) and terrestrial (organic matter, absence of macrofossils) productivity throughout LGM age sediments at Harding Lake indicate generally dry and cold conditions with a short ice free (growing) season. Accordingly, proxy evidence from Harding Lake contradict the climate model simulation conclusions of Otto-Bliesner et al. (2006) and pollen based climate reconstructions of Bartlein et al. (2011). This apparent discrepancy may result from contrasting seasonal influences, whereby lacustrine proxies are responding to summer, growing season conditions. Mean annual temperatures in interior Alaska during the LGM, on the other hand, may be more influenced by winter season temperature variability.

5.3. The Lateglacial and early Holocene (15,700–9,400 yr BP)

The abrupt increase in organic matter and biogenic silica concentration at 15,700 yr BP marks the transition into the Lateglacial and indicates wetter conditions at Harding Lake. A corresponding decrease in dry bulk density, magnetic susceptibility, and titanium values further suggests a decrease in windiness and ameliorating climatic conditions (Fig. 6). The intermediate organic matter and biogenic silica content of Unit 2 sediments suggests that although aquatic and terrestrial productivity levels were higher than before, they were still lower than modern levels. These results combined with a subtle increase in the sedimentation rate as well as lower magnetic susceptibility and titanium values imply that lake levels were higher relative to Unit 1. Rising and high *Betula* (>50%) pollen and a corresponding decline in herb taxa beginning shortly before 14,600 yr BP (Fig. 7) further suggests that climatic conditions were warmer and wetter compared to the LGM. Comparison with other AMS dated lake records from interior Alaska show the *Betula* rise occurred between 13,500 and 14,000 yr BP at Jan Lake (Carlson and Finney, 2004) and Birch Lake (Bigelow, 1997), and thus suggest the *Betula* rise occurred contemporaneously or slightly earlier at Harding Lake. Collectively, proxy and core-transect evidence indicates a rapid lake level rise beginning at 15,700 yr BP reaching above 17 m BML by ~14,000 yr BP (Fig. 10A). The presence of an erosional unconformity in core E–12 demonstrates that lake level fluctuated or dropped after the initial rise. Regardless, the preservation of lacustrine sediment above this interval provides evidence that lake-levels did not drop below 17 m BML again for any sustained time.

The proxy data from Harding Lake support existing evidence for significant climatic change during the Lateglacial in Alaska. For example, a pollen based reconstruction for eastern Beringia (Viau et al., 2008) indicates rising mean annual temperatures beginning around 16,000 yr BP and peak Lateglacial mean annual temperatures by 12,000 yr BP. The onset of inferred warming at Harding Lake occurred during a time of increasing summer insolation (Fig. 10C; Berger and Loutre, 1991) and rapid deglaciation in the Alaska Range (eg. Young et al., 2009). Notably, the Lateglacial transition at Harding Lake also corresponds to a rapid 18 m lake level rise at Birch Lake at ~15,000 yr BP (Fig. 10B; Abbott et al., 2000), suggesting that climate was substantially wetter than before. This assertion is supported by evidence that numerous small lakes began accumulating lacustrine sediment between 15,000 and 13,000 yr BP in lowland central Alaska (eg. Ager, 1983; Bigelow, 1997; Carlson and Finney, 2004) as well as evidence for deglaciation and warmer temperatures in the lower Fish Lake valley (located in the northeastern Alaska Range) by 15,000–14,000 yr BP (Young et al., 2009).

Marine sediments from the southeastern Bering Sea (HLY0502-51JPC) do not contain detectable amounts of C_{37} alkenones prior to ~16,700 yr BP (Cassie et al., 2010), implying perennial sea ice cover during the LGM. Alkenone derived sea surface temperature estimates and diatom assemblage data indicate warming sea surface temperatures and a transition from sea-ice to open water species during the Lateglacial period (Cassie et al., 2010). In general, the available evidence from Harding Lake and comparison with other paleoproxy records shows the Lateglacial was a time of wetter and warmer conditions, compared to the LGM, in central Alaska.

5.4. The early to middle-Holocene (9,400–8,700 yr BP)

The abrupt increase in organic matter and biogenic silica content (Fig. 6) along with the highest sedimentation rates (0.225 cm/yr) of the entire record (Fig. 4), and the simultaneous decline in magnetic susceptibility and titanium content indicate that considerable climatic and environmental changes occurred at Harding Lake at 9,400 yr BP. We suggest the abrupt change in the sediment physical and geochemical data signifies rapidly rising and much higher lake levels between 9,400 and 8,700 yr BP. This interpretation is consistent with the accumulation of lacustrine sediment above the erosional unconformity in core E-12 by 9,660 yr BP. The marked increase in organic matter and biogenic silica can be attributed to a further increase in precipitation and rising lake levels, along with an increase in the length of the summer ice-free season from warmer temperatures associated with the summer insolation maxima (Berger and Loutre, 1991). The increase in biogenic silica is likely also caused, in part, by increased availability of nutrients and autochthonous organic sediment flux. Continued predominance of *Betula* (>50%) pollen, along with a concomitant

decline in herb taxa and subtle increase in *Sphagnum* and *Isoetes* at 9,100 yr BP (Fig. 7), further demonstrate increasingly wet conditions and higher lake levels. The corresponding decrease in titanium and magnetic susceptibility represents the final transition to interglacial climatic conditions, wherein a generally stable climate characteristic of the Holocene prevailed.

The Harding Lake sediment signal at 9,400 yr BP is explainable in the context of numerous other terrestrial records from central Alaska that demonstrate an increase in precipitation and potentially warmer conditions. Sedimentary evidence from Birch Lake shows rising lake levels to near the overflow level between 10,000 and 9,000 yr BP (Fig. 10B; Abbott et al., 2000). Rising lake-levels also occurred at this time at Marcella Lake in the southwest Yukon (Anderson et al., 2005) and after 9,500 yr BP at Dune Lake (Finney et al., 2012). In addition, this period broadly corresponds with the early Holocene peak in summer insolation (Fig. 10C; Berger and Loutre, 1991) as well as rising sea levels (Fig. 10D) and the final submergence of the Bering land bridge (Elias et al., 1996), which would have reduced the transport distance of warm, moist North Pacific air masses traveling towards interior Alaska. Nevertheless, the gradual change in insolation forcing and eustatic sea level rise during this interval precludes a direct linkage between these forcings and the sediment anomaly. We therefore suggest the rapid changes in sedimentation at Harding Lake likely reflect an abrupt (and probably temporary) change in atmospheric circulation, possibly associated with further retreat of the Laurentide Ice Sheet.

5.5. The middle to late-Holocene (8,700 yr BP to present, 2010 AD)

Proxy evidence from Harding Lake suggests that water levels were generally high (Fig. 10A) for the remainder of the Holocene. The decline in sedimentation rates to lower and stable Holocene levels (0.015–0.04 cm/yr), along with the subtle increase and peak in magnetic susceptibility and titanium by 7,100 yr BP implies that lake levels were higher and that shoreline reworking provided a source of minerogenic sediments to the lake depocenter. The remainder of Holocene sediment is characterized by low and declining magnetic susceptibility and titanium values. The appearance of *Alnus* and *Picea* between 8,600 and 7500 yr BP (Fig. 7), and later increases in *Alnus* by 7,000 yr BP and *Picea* by 5,600 yr BP, respectively, indicate development of coniferous forest quite similar to present and further imply warm and wet conditions. *Isoetes* predominates the aquatic taxa and *Myriophyllum* is absent, consistent with deeper water at the depocenter (eg. Edwards et al., 2000). The higher organic matter content and generally low and declining magnetic susceptibility (Fig. 6) values suggest relatively high lake levels through the middle to late Holocene. Substantially lower magnetic susceptibility values suggest that sediment composition in this interval is relatively insensitive to further low magnitude lake-level changes (Fig. 9A). A gradual trend toward higher C/N ratios indicates organic matter increasingly originated from terrestrial sources during the middle to late Holocene (Fig. 6). In addition, organic matter $\delta^{13}C$ values gradually increase (Fig. 6) becoming more enriched, and combined with higher organic matter content, suggest increasing levels of aquatic productivity within Harding Lake. Notably, biogenic silica concentrations peak during the mid-Holocene between 5,500 and 3,100 yr BP and fluctuate at millennial time scales (Fig. 6). Given that magnetic susceptibility and titanium values are generally stable and decreasing throughout the Holocene (with minimal evidence of diatom dissolution), we attribute the variability in biogenic silica content to fluctuations in aquatic productivity.

Unchanging to overflowing lake levels persisted from ~6,000 yr BP to the present at Birch Lake (Fig. 9B; Abbott et al., 2000), suggesting the middle to late Holocene climate of central Alaska was generally moist and stable. Core transect data from Jan Lake in the middle Tanana Valley suggest rising lake levels from 9,000 yr BP to the present, indicating a trend towards wetter conditions through the Holocene (Barber and Finney, 2000). Historical observations from Harding Lake demonstrate lake level fluctuations on the order of several meters since the 1930's (LaPerriere, 2003), with periodic exposure of the shallow shelf along the northern shore. Given the substantial water depth of the depocenter at Harding Lake (>42 m), this deep core site appears relatively insensitive to recent low-magnitude lake level fluctuations.

6. Conclusions

A multi-proxy geochemical investigation of sediments from Harding Lake in interior Alaska reveal millennial scale changes in lake level, vegetation patterns, and paleoclimate over the last 31,000 yr BP. Detailed analysis of core sedimentology along with AMS radiocarbon dates on terrestrial macrofossils from a depocenter core (42 m water depth) collectively indicate Harding Lake persisted as a shallow, low productivity lake during the LGM, a known period of extreme aridity. The general absence of terrestrial macrofossils for radiocarbon dating and low organic matter and biogenic silica content suggest sparse terrestrial vegetation in the vicinity and low in-lake productivity. Pollen data show a predominance of herb taxa during this time that is likely indicative of tundra conditions. An increase in organic matter and biogenic silica content at 15,700 yr BP marks the transition into the Lateglacial and indicates rising lake levels at Harding Lake and variable hydroclimatic conditions thereafter until 9,400 yr BP. Core transect data confirm a substantial lake-level rise with the onset of lacustrine sedimentation at 17.1 m BML by ~14,000 yr BP and lower or fluctuating lake-levels thereafter until 9,400 yr BP. Combined with evidence for a decrease in windiness (lower magnetic susceptibility and titanium) and expansion of *Betula* forest at 14,600 yr BP, the proxy data indicate wetter and potentially warmer conditions. A rapid increase in sedimentation rate and rising organic matter and biogenic silica content with a simultaneous decline in magnetic susceptibility and titanium values indicate that considerable environmental changes occurred at Harding Lake between 9,400 and 8,700 yr BP. Core transect data and composite core proxy evidence suggests rapidly rising and much higher lake levels than at any previous time during the record. The increase in organic matter and biogenic silica is attributed to a further increase in the length of the summer ice-free season and high nutrient loads, while declining titanium and magnetic susceptibility resulted from the final transition to interglacial climatic conditions. High *Betula* pollen and a minor component of *Sphagnum* and *Isoetes* indicate wetter conditions and higher lake-levels. This period of rapid environmental change broadly corresponds to the submergence of the Bering land bridge and early Holocene maxima in summer insolation; however the abruptness of this transition precludes a direct linkage from insolation forcing and sea level rise. We alternatively suggest the rapid changes in sedimentation at Harding Lake beginning at 9,400 yr BP likely reflect an abrupt change in atmospheric circulation, possibly associated with further retreat of the Laurentide Ice Sheet and wetter conditions in interior Alaska. A return to stable and lower sedimentation rates by 8,700 yr BP, along with higher organic matter and low magnetic susceptibility, suggest generally high and stable lake levels over the middle to late-Holocene with conditions similar to the modern lake. Increases in *Alnus* by 7,000 yr BP and *Picea* by 5,600 yr BP, combined with continued predominance of *Betula* through the Holocene, indicate substantial expansion of forest around Harding Lake.

The use of AMS radiocarbon dating of terrestrial macrofossils and higher resolution proxy analysis relative to a previous study of

Harding Lake sediments provide a better understanding of both the timing and magnitude of late-Quaternary climate variability in interior Alaska. Analysis of both a depocenter core and transect of cores from varying depths demonstrate that lake level reconstructions using a combination of methods are more robust than a single core approach, and provide quantitative information regarding past hydroclimate variability. Further, deep lake basins in the unglaciated interior of Alaska preserve older sedimentary records than small, shallow lakes and therefore provide an important terrestrial archive to investigate paleoenvironmental change across the LGM to Holocene transition.

Acknowledgments

Funding for this project was provided by the National Science Foundation (ARC-0908200, ARC-0909310) and the Henry Leighton Memorial Graduate Scholarship through the University of Pittsburgh Department of Geology and Planetary Science. We thank Adele Virgin, Christopher Purcell, Jason Addison, Bernie Baecker and Dave Pompeani for assistance in the field; Nancy Bigelow for use of coring equipment during the July 2012 field season; John Southon, Guaciarra dos Santos and prep-lab personnel (Hector Martinez, Chanda Bertrand, and Shari Bush) at the Keck Carbon Cycle Accelerator Mass Spectrometry Laboratory at the University of California, Irvine for assistance in preparing graphite targets and isotope measurement for radiocarbon analysis; and Aubrey Hillman and Kaitlyn Clark for help with the research. This manuscript was greatly improved by the helpful suggestions from two anonymous reviewers.

References

Abbott, M.B., Stafford, T.W., 1996. Radiocarbon geochemistry of ancient and modern lakes, Arctic lakes, Baffin Island. Quat. Res. 45, 300–311.
Abbott, M.B., Finney, B.P., Edwards, M.E., Kelts, K.R., 2000. Lake-level reconstructions and paleohydrology of Birch Lake, central Alaska, based on seismic reflection profiles and core transects. Quat. Res. 53, 154–166.
Abbott, M.B., Edwards, M.E., Finney, B.P., 2010. A 40,000-yr record of environmental change from Burial Lake in Northwest Alaska. Quat. Res. 74, 156–165.
Ager, T.A., 1975. Late Quaternary Environmental History of the Tanana Valley, Alaska. Institute of Polar Studies, Report No. 54. Ohio State University, Columbus, p. 117.
Ager, T.A., 1983. Holocene vegetational history of Alaska. In: Wright Jr., (Ed.), Late Quaternary Environments of the United States, The Holocene, vol. 2. University of Minnesota Press, Minneapolis, pp. 128–141.
Anderson, L., Abbott, M.B., Finney, B.P., Edwards, M.E., 2005. Palaeohydrology of the Southwest Yukon Territory, Canada, based on multiproxy analyses of lake sediment cores from a depth transect. Holocene 15 (8), 1172–1183.
Barber, V.A., Finney, B.P., 2000. Late Quaternary paleoclimatic reconstructions for interior Alaska based on paleolake-level data and hydrologic models. J. Paleolimnol. 24, 29–41.
Balascio, N.L., Bradley, R.S., 2012. Evaluating Holocene climate change in northern Norway using sediment records from two contrasting lake systems. J. Paleolimnol. 48, 259–273.
Bartlein, J.P., Anderson, P.M., Edwards, M.E., McDowell, P.F., 1991. A framework for interpreting paleoclimatic variations in eastern Beringia. Quat. Int. 10, 73–83.
Bartlein, P.J., Harrison, S.P., Brewer, S., Connor, S., Davis, B.A.S., Gajewski, K., Guiot, J., Harrison-Prentice, T.I., Henderson, A., Peyron, O., Prentice, I.C., Scholze, M., Seppä, H., Shuman, B., Sugita, S., Thompson, R.S., Viau, A.E., Williams, J., Wu, H., 2011. Pollen-based continental climate reconstructions at 6 and 21 ka: a global synthesis. Clim. Dyn. 37 (3), 775–802.
Berger, A., Loutre, M.F., 1991. Insolation values for the climate of the last 10 million years. Quat. Sci. Rev. 10 (4), 297–317.
Bigelow, N.H., 1997. Late-Quaternary Climate and Vegetation in Interior Alaska (PhD dissertation). University of Alaska, Fairbanks.
Bigelow, N.H., Edwards, M.E., 2001. A 14,000 yr paleoenvironmental record from Windmill Lake, Central Alaska: evidence for high-frequency climatic and vegetation fluctuations. Quat. Sci. Rev. 20, 203–215.
Binford, M.W., 1990. Calculation and uncertainty analysis of ^{210}Pb dates for PIRLA project sediment cores. J. Paleolimnol. 3, 253–267.
Blaauw, M., 2010. Methods and code for 'classical' age-modeling of radiocarbon sequences. Quat. Geochronol. 5, 512–518.
Blackwell, J., 1965. Surficial Geology and Geomorphology of the Harding Lake Area, Big Delta Quadrangle, Alaska (Masters thesis). University of Alaska, Fairbanks.
Briner, J.P., Kaufman, D.S., 2000. Late Pleistocene glaciation of the southwestern Ahklun Mountains, Alaska. Quat. Res. 53, 13–22.
Briner, J.P., Kaufman, D.S., Manley, W.F., Finkel, R.C., Caffee, M.W., 2005. Cosmogenic exposure dating of late Pleistocene moraine stabilization in Alaska. Geol. Soc. Am. Bull. 117, 1108–1120.
Carlson, L.J., Finney, B.P., 2004. A 13,000-year history of vegetation and environmental change at Jan Lake, east-central Alaska. Holocene 14 (6), 818–827.
Cassano, E.N., Cassano, J.J., Nolan, M., 2011. Synoptic weather pattern controls on temperature in Alaska. J. Geophys. Res. 116 (12), D11108.
Cassie, B.E., Brigham-Grette, J., Lawrence, K.T., Herbert, T.D., Cook, M.S., 2010. Last Glacial Maximum to Holocene sea surface conditions at Umnak Plateau, Bering Sea, as inferred from diatom, alkenone, and stable isotope records. Paleoceanography 25, PA1206.
COHMAP Members, 1988. Climatic changes of the last 18,000 years: observations and model simulations. Science 241, 1043–1053.
Coulter, H.W., Hopkins, D.M., Karlstrom, T.N.V., Péwé, T.L., Wahrhaftig, C., Williams, J.R., 1965. Map Showing Extent of Glaciations in Alaska. U.S. Geological Survey. Map, I-415.
Croudace, I.W., Rindby, A., Rothwell, R.G., 2006. ITRAX: description and evaluation of a new multi-function X-ray core scanner. In: New Techniques in Sediment Core Analysis. Geological Society, London, Special Publications, vol. 267, pp. 51–63.
Edwards, M.E., Bigelow, N.H., Finney, B.P., Eisner, W.R., 2000. Records of aquatic pollen and sediment properties as indicators of late-Quaternary Alaskan lake levels. J. Paleolimnol. 24, 55–68.
Elias, S.A., Short, S.K., Nelson, C.H., Birks, H.H., 1996. Life and times of the Bering Land Bridge. Nature 382, 60–63.
Elias, S.A., Hamilton, T.D., Edwards, M.E., Begét, J.E., Krumhardt, A.P., Lavoie, C., 1999. Late Pleistocene environments of the western Noatak Basin, northwestern Alaska. Geol. Soc. Am. Bull. 111, 769–789.
Faegri, K., Kaland, P.E., Krzywinski, K., 1989. Textbook of Pollen Analysis, fourth ed. Wiley, New York.
Finney, B.P., Bigelow, N.H., Barber, V.A., Edwards, M.E., 2012. Holocene climate change and carbon cycling in a groundwater-fed, boreal forest lake, Dune Lake, Alaska. J. Paleolimnol. 48, 43–54.
Grimm, E.C., 1990. TILIA and TILIA*GRAPH. PC spreadsheet and graphics software for pollen data. INQUA Working Group on Data-Handling Methods. Newsletter 4, 5–7.
Hamilton, T.D., Craig, J.L., Sellman, P.V., 1988. The Fox permafrost tunnel: a late Quaternary geologic record in central Alaska. Geological Soc. Am. Bull. 100, 948–969.
Heiri, O., Lotter, A.F., Lemcke, G., 2001. Loss on ignition as a method for estimating organic and carbonate content in sediments: reproducibility and comparability of results. J. Paleolimnol. 25, 101–110.
Hopkins, D.M., 1982. Aspects of the paleogeography of Beringia during the Late Pleistocene. In: Hopkins, D.M., Matthews, J.V., Schweger, C.E., Young, S.B. (Eds.), Paleoecology of Beringia. Academic Press, New York, pp. 3–28.
Hu, F.S., Brubaker, L.B., Anderson, P.M., 1993. A 12,000 year record of vegetation change and soil development from Wien Lake, central Alaska. Can. J. Bot. 71 (9), 1133–1142.
Hu, F.S., Brubaker, L.B., Anderson, P.M., 1996. Boreal ecosystem development in the northwestern Alaska Range since 11,000 yr B.P. Quat. Res. 45, 188–201.
Hu, F.S., Finney, B.P., Brubaker, L.B., 2001. Effects of Holocene Alnus expansion on aquatic productivity, nitrogen cycling, and soil development in southwestern Alaska. Ecosystems 4, 358–368.
Jorgenson, M.T., Yoshikawa, K., Kanveskiy, M., Shur, Y.L., Romanovsky, V., Marchenko, S., Grosse, G., Brown, J., Jones, B., 2008. Permafrost characteristics of Alaska. In: Kane, D.L., Hinkel, K.M. (Eds.), Proceedings of the Ninth International Conference on Permafrost, 29 June – 3 July 2008, Fairbanks, Alaska. Institute of Northern Engineering, University of Alaska Fairbanks, pp. 121–122.
Kaufman, D.S., Young, N.E., Briner, J.P., Manley, W.F., 2011. Alaska Paleo glacier Atlas version 2. In: Ehlers, J., Gibbard, P.L. (Eds.), Quaternary Glaciations – Extent and Chronology: North America, Developments in Quaternary Sciences, vol. 15, pp. 427–445.
LaPerriere, J.D., 2003. Limnology of Harding Lake, Alaska: a deep, subarctic lake. Lake Reserv. Manag. 19, 93–107.
Matmon, A., Briner, J.P., Carver, G., Bierman, P., Finkel, R., 2010. Moraine chronosequence of the Donnelly Dome region, Alaska: implications for the late Pleistocene glacial history of interior Alaska. Quat. Res. 74, 63–72.
Matthews, J.V., 1974. Wisconsin environment of interior Alaska: pollen and macrofossil analysis of a 27 meter core from the Isabella Basin (Fairbanks, Alaska). Can. J. Earth Sci. 11, 828–841.
Mock, C.J., Bartlein, P.J., Anderson, P.A., 1998. Atmospheric circulation patterns and spatial climatic variations in Beringia. Int. J. Climatol. 10, 1085–1104.
Mortlock, R.A., Froelich, P.N., 1989. A simple method for the rapid determination of biogenic opal in pelagic marine sediments. Deep-Sea Res. 35, 1415–1426.
Muhs, D.R., Ager, T.A., Bettis III, E.A., McGeehin, J., Been, J.M., Beg!et, J.E., Pavich, M.J., Stafford Jr., T.W., Stevens, D.S.P., 2003. Stratigraphy and palaeoclimatic significance of Late Quaternary loess-palaeosol sequences of the Last-Interglacial-Glacial cycle in central Alaska. Quat. Sci. Rev. 22, 1947–1986.
Nakao, K., Tanoue, R., Yokoyama, T., 1981. Origin of Harding Lake in interior Alaska. J. Fac. Sci. Hokkaido Univ. 7 (1), 1–12.
Nakao, K., Ager, T.A., 1985. Climatic changes and vegetational history of the interior of Alaska inferred from drilled cores at Harding Lake. In: Nakao, K. (Ed.), Hydrological Regime and Climatic Changes in the Arctic Circle. Report of the

Alaskan Paleohydrology Research Project, Laboratory of Hydrology, Department of Geophysics, Faculty of Science, Hokkaido University, Japan.
Oswald, W.W., Anderson, P.M., Brown, T.A., Brubaker, L.B., Hu, F.S., Lozhkin, A.V., Tinner, W., Kaltenrieder, P., 2005. Effects of sample mass and macrofossil type on radiocarbon dating of arctic and boreal lake sediments. Holocene 15 (5), 758–767.
Otto-Bliesner, B.L., Brady, E.C., Clauzet, G., Tomas, R., Levis, S., Kothavala, Z., 2006. Last Glacial Maximum and Holocene climate in CCSM3. J. Clim. 19, 2526–2544.
Péwé, T.L., 1975. The Quaternary Geology of Alaska. In: USGS Professional Paper, vol. 385, p. 145.
Peltier, W.R., Fairbanks, R.G., 2006. Global glacial ice volume and LGM duration from an extended Barbados sea level record. Quat. Sci. Rev. 25, 3322–3337.
Pompeani, D.P., Steinman, B.A., Abbott, M.B., 2012. A sedimentary and geochemical reconstruction of water level changes from Rantin Lake, Yukon, Canada. J. Paleolimnol. 48, 147–158.
Reimer, P.J., Baillie, M.G.L., Bard, E., Bayliss, A., Beck, J.W., Blackwell, P.G., Bronk Ramsey, C., Buck, C.E., Burr, G.S., Edwards, R.L., Friedrich, M., Grootes, P.M., Guilderson, T.P., Hajdas, I., Heaton, T.J., Hogg, A.G., Hughen, K.A., Kaiser, K.F., Kromer, B., McCormac, F.G., Manning, S.W., Reimer, R.W., Richards, D.A., Southon, J.R., Talamo, S., Turney, C.S.M., van der Plicht, J., Weyhenmeyer, C.E., 2009. IntCal09 and Marine09 radiocarbon age calibration curves, 0-50,000 years cal BP. Radiocarbon 51, 1111–1150.
Santos, G.M., Southon, J.R., Drenzek, N.J., Ziolkowski, L.A., Druffel, E., Xu, X., Zhang, D., Trumbore, S., Eglington, T.I., Hughen, K.A., 2010. Blank assessment for ultra-small radiocarbon samples: chemical extraction and separation versus AMS. Radiocarbon 52 (2–3), 1322–1335.
Schnurrenberger, D., Russell, J., Kelts, K., 2003. Classification of lacustrine sediments based on sedimentary components. J. Paleolimnol. 29 (2), 141–154.
Stafford, J.M., Wendler, G., Curtis, J., 2000. Temperature and precipitation of Alaska: 50 year trend analysis. Theor. Appl. Climatol. 67, 33–44.
Stansell, N.D., Abbott, M.B., Rull, V., Rodbell, D.T., Bezada, M., Montoya, E., 2010. Abrupt Younger Dryas cooling in the northern tropics recorded in lake sediments from the Venezuelan Andes. Earth Planet. Sci. Lett. 293, 154–163.
Streten, N.A., 1974. Some features of the summer climate of interior Alaska. Arctic 27, 272–286.
Viau, A.E., Gajewski, K., Sawada, M.C., Bunbury, J., 2008. Low- and high-frequency climate variability in eastern Beringia during the past 25,000 years. Can. J. Earth Sci. 45, 1435–1453.
Waelbroeck, C., Labeyrie, L., Michel, E., Duplessy, J.C., McManus, J., Lambeck, K., Balbon, E., Labracherie, M., 2002. Sea-level and deep water temperature changes derived from benthic foraminifera isotopic records. Quat. Sci. Rev. 21, 295–305.
Wahrhaftig, C., 1965. Physiographic Divisions of Alaska. In: U.S. Geological Survey Professional Paper, vol. 482. U.S. Geological Survey, p. 52.
Wilson, F.H., Dover, J.H., Bradley, D.C., Weber, F.R., Bundtzen, T.K., Haeussler, P.J., 1998. Geologic Map of Central (Interior) Alaska. U.S. Geological Survey Open-File Report OF 98–133. U.S. Geological Survey, p. 64.
Wooller, M.J., Kurek, J., Gaglioti, B.V., Cwynar, L.C., Bigelow, N., Reuther, J.D., Gelvin-Reymiller, C., Smol, J.P., 2012. An 11,200 year paleolimnological perspective for emerging archeological findings at Quartz Lake, Alaska. J. Paleolimnol. 48, 83–99.
Young, N.E., Briner, J.P., Kaufmann, D.S., 2009. Late Pleistocene and Holocene glaciation of the Fish Lake valley, northeastern Alaska Range, Alaska. J. Quat. Sci. 24 (7), 677–689.